DOI: 10.1002/ejic.201100184

Lanthanide Carbonates

Rafał Janicki,[a] Przemysław Starynowicz,[a] and Anna Mondry*[a]

Keywords: Structure elucidation / UV/Vis/NIR spectroscopy / IR spectroscopy / Density functional calculations / Lanthanides / Carbonate complexes

The crystal and molecular structures of the rare earth carbonates with the general formulae $[C(NH_2)]_3[Ln(CO_3)_4(H_2O)]\cdot 2H_2O$ (where Ln = Pr^{3+}, Nd^{3+}, Sm^{3+}, Eu^{3+}, Gd^{3+}, Tb^{3+}) and $[C(NH_2)]_3[Ln(CO_3)_4]\cdot 2H_2O$ (where Ln = Y^{3+}, Dy^{3+}, Ho^{3+}, Er^{3+}, Tm^{3+}, Yb^{3+}, Lu^{3+}) were determined. The crystals consist of monomeric $[Ln(CO_3)_4(H_2O)]^{5-}$ or $[Ln(CO_3)_4]^{5-}$ complex anions in which the carbonate ligands coordinate to the Ln^{3+} ion in a bidentate manner. The spectroscopic (UV/Vis/NIR and IR) properties of the crystalline lanthanide carbonates, as well as their aqueous solutions, were determined. Correlation between the spectroscopic and the structural data enabled us to conclude that the $[Ln(CO_3)_4(OH)]^{6-}$ and $[Ln(CO_3)_4]^{5-}$ species predominate in the light and heavy lanthanide solutions, respectively. The nature of the Ln–O interaction was also discussed. The experimental data, as well as the theoretical calculations, indicated that the Ln–O(CO_3^{2-}) bond is more covalent than the Ln–O(OH_2) bond. Moreover, the covalency degree is larger for the heavy lanthanide ions. Inspection of the NBO results revealed that the oxygen hybrids, with the approximate composition sp^4, form strongly polarized bonds with the $6s6p5d^4$ hybrids of lutetium.

Introduction

The lanthanide complexes with carbonate anions have been studied for several years.[1] These complexes have a potential practical role, for example, the common and cheap carbonate anions may be used to separate lanthanide and actinide ions from the nuclear waste.[2]

It is well known that lanthanides, as well as actinides, form soluble, thermodynamically-stable, highly charged anionic species in concentrated solutions of alkali metal carbonates. The substantial stability of these complexes is brought about by the high basicity of the CO_3^{2-} anion and the large effective charge of the Ln^{3+} cations. The cumulative stability constants of the $[Ln(CO_3)_n]^{-2n+3}$ complexes, which have been determined by various methods (i.e. potentiometry, solubility and extraction), are widely discussed.[3] The stoichiometry of the lanthanide carbonate complexes significantly differ and depend on the experimental conditions. The presence of 1:1 and 1:2 complexes[4] is expected in dilute solutions of the carbonate anion (e.g. sea water) while the $[Ln(CO_3)_3]^{3-}$[5] and $[Ln(CO_3)_4]^{5-}$[6] species are formed in concentrated solutions. The UV/Vis spectroscopy results reported by Nagaishi et al.[6] indicated that the eight-coordinate $[Ln(CO_3)_4]^{5-}$ (where Ln = Nd^{3+}, Sm^{3+}, Eu^{3+}, Gd^{3+}, Tb^{3+}, Dy^{3+}, and Tm^{3+}) species were predominant in a 3 M K_2CO_3 aqueous solution. This conclusion is in agreement with the results obtained by Rao and Chatt[4a] (solvent extraction), as well as by Bond et al.[7] (IR and Raman spectroscopy). On the other hand, the measurements of the electrophoretic mobilities and solubilities of $Na[Eu(CO_3)_2]\cdot nH_2O$, which was performed by Philippini et al.,[8,9] indicated different complex stoichiometries for the light ($[Ln(CO_3)_4]^{5-}$) and heavy ($[Ln(CO_3)_3]^{3-}$) lanthanides. These differences were explained by the lanthanide contraction. Vercouter et al.,[5,9] by taking into account the results from the solubility and time-resolved laser-induced fluorescence spectroscopy (TRLFS) studies, concluded that the 8-coordinate $[Eu(CO_3)_3(H_2O)_2]^{3-}$ species was predominant in solution.

Some interesting properties of the lanthanide carbonate complexes were observed by Hobart et al.[10] They found that it is possible to oxidize electrochemically trivalent praseodymium and terbium to the tetravalent state in alkali carbonate solutions ($c_{K_2CO_3}$ = 5.5 M). This suggests that the coordination environment of the Ln^{3+} ion is completely filled up by the carbonate anions.

The number of reported crystal structure analyses of Ln carbonates is limited,[7,11–20] since these compounds, in most cases, have been synthesized hydrothermally in the form of powders.[21,22] In the majority of reported crystal structures, the coordination sphere of the Ln^{3+} ion consists only of the carbonate anions. The coordination number (C.N.) of the metal ion is 9 for the light lanthanides and 9 or 8 for the heavy lanthanides. A C.N. of 10 was found for a holmium complex,[11] in which the Ho^{3+} ion was surrounded by three bidentate HCO_3^- anions and four water molecules.

[a] Faculty of Chemistry, University of Wrocław,
F. Joliot-Curie 14, 50-383 Wrocław, Poland
Fax: +48-71-3282348
E-mail: anm@wchuwr.pl

Supporting information for this article is available on the WWW under http://dx.doi.org/10.1002/ejic.201100184.

Despite a great amount of research on lanthanide carbonates, there is a lack of systematic structural and spectroscopic studies of these complexes for all of the lanthanide ions and, in particular, for single crystals that have been obtained at the same experimental conditions.

Electronic spectroscopy is the method of choice to study lanthanide complexes in solution.[23] This is particularly true in the case of lanthanide carbonates, where very high ionic strengths of the investigated solutions impede the use of other physicochemical methods. Moreover, the correlation between the UV/Vis/NIR absorption spectra of monocrystals and solutions seems to be an especially valuable method, which enables to determine stoichiometry and structure of the complex in solution, as the specific character of f–f transitions, namely their intensity variations and crystal-field splittings, depend mainly on the nearest sourrounding of Ln^{3+}.[23]

Systematic analysis of the structural and spectroscopic properties of the rare earth (Pr^{3+}, Nd^{3+}, Sm^{3+}, Eu^{3+}, Gd^{3+}, Tb^{3+} Dy^{3+}, Ho^{3+}, Er^{3+}, Tm^{3+}, Yb^{3+}, Lu^{3+}, and Y^{3+}) carbonate complexes is presented in this paper. Correlation of the spectral properties between complexes in the solid state and in solution is also analyzed. This study should be of interest as the observed physicochemical properties of the lanthanide carbonates may shed some light on the debated nature of the Ln–O bond.[24]

Results

Crystal Structures

The complexes with the formulae $[C(NH_2)]_3[Ln(CO_3)_4(H_2O)]\cdot 2H_2O$ (**I**) (where Ln = Pr^{3+}, Nd^{3+}, Sm^{3+}, Eu^{3+}, Gd^{3+}, Tb^{3+}) and $[C(NH_2)]_3[Ln(CO_3)_4]\cdot 2H_2O$ (**II**) (where Ln = Y^{3+}, Dy^{3+}, Ho^{3+}, Er^{3+}, Tm^{3+}, Yb^{3+}, Lu^{3+}) crystallize in the $Pna2_1$ and *Pnna* space groups, respectively. The crystals of **I** are isostructural with the previously studied Nd^{3+} compound.[13] In both types of crystals, four bidentate carbonate anions coordinate to the Ln^{3+} ion, thus filling the eight coordination sites. The ninth coordination place in **I** is occupied by a water molecule, as shown in Figure 1.

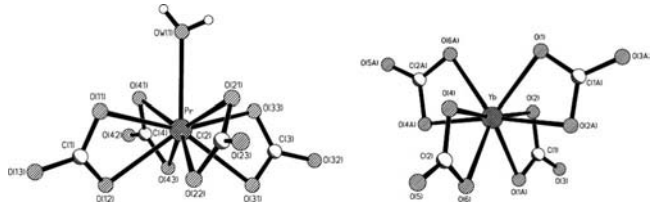

Figure 1. The molecular structure of $[Pr(CO_3)_4(H_2O)]^{5-}$ and $[Yb(CO_3)_4]^{5-}$ together with the atom labels.

In **I**, the eight oxygen atoms from the carbonate anions and a water molecule form a distorted monocapped square antiprism (*SAPRS*-9) in which the bases are twisted by 23°. In **II**, the eight carbonate oxygen atoms form a distorted dodecahedron (*DD*-8). The molecular symmetry of the complex anions is rather low, namely, C_1 in **I** and C_{2v} in **II**. The Ln–O bond lengths are presented in Table 1. They are comparable to those previously reported in the literature;[7,15,17] the Y–O bond lengths are intermediate between those of the Ho and Er crystals. The rest of the details of the data collection and the structure refinement are given in Tables S1 and S2. The change in the average bond lengths for the Ln–O(CO_3^{2-}), Ln–OH_2, and Ln–Ln distances across the lanthanide series are presented in Figure 2.

The discontinuity in the Ln–Ln bond lengths between the Tb and Dy compounds was caused by the change in the C.N. from 9 for Tb^{3+} to 8 for Dy^{3+}. The difference between the Ln–OH_2 bond lengths for Eu^{3+}, Gd^{3+}, and Tb^{3+} in **I** was caused by the formation of hydrogen bonds between the coordinated water molecule, OW1, and one of the two alternative acceptor oxygen atoms. In the Pr^{3+}, Nd^{3+}, Sm^{3+}, and Eu^{3+} compounds, the OW1 molecule forms a hydrogen bond with the oxygen atom (O12) from an adjacent com-

Table 1. Ln–O bond lengths (Å) for **I** and **II**. The estimated standard deviations of the sample are given in the case of the average distances.

	$[Ln(CO_3)_4(H_2O)]^{5-}$						
	Pr^{3+}	Nd^{3+}	Sm^{3+}	Eu^{3+}	Gd^{3+}	Tb^{3+}	
Ln–O33	2.4741(17)	2.455(2)	2.4219(16)	2.410(3)	2.393(5)	2.383(3)	
Ln–O21	2.4753(18)	2.463(2)	2.4269(16)	2.414(3)	2.409 (5)	2.388(3)	
Ln–O41	2.4828(17)	2.4669(19)	2.4342(15)	2.423(3)	2.422(4)	2.404(3)	
Ln–O11	2.4877(18)	2.471(2)	2.4403(16)	2.427(3)	2.397(5)	2.396(3)	
Ln–O31	2.5042(18)	2.485(2)	2.4563(15)	2.441(3)	2.446(4)	2.438(3)	
Ln–O12	2.5074(16)	2.4897(18)	2.4617(15)	2.448(3)	2.432(5)	2.436(4)	
Ln–O22	2.5279(17)	2.513(2)	2.4871(16)	2.476(3)	2.462(5)	2.458(3)	
Ln–O43	2.5618(17)	2.5449(19)	2.5231(15)	2.516(3)	2.506(5)	2.490(3)	
Average	2.502(30)	2.486(30)	2.456(34)	2.444(35)	2.436(40)	2.424(38)	
Ln–OW1	2.503(30)	2.486(30)	2.456(34)	2.444(36)	2.433(38)	2.424(38)	
	$[Ln(CO_3)_4]^{5-}$						
	Dy^{3+}	Ho^{3+}	Er^{3+}	Tm^{3+}	Yb^{3+}	Lu^{3+}	Y^{3+}
Ln–O4	2.3601(13)	2.3438(12)	2.3265(15)	2.3192(15)	2.3102(12)	2.2992(13)	2.339(2)
Ln–O1	2.356(11)	2.3440(11)	2.3334(16)	2.3225(15)	2.3132(11)	2.3071(11)	2.3441(18)
Ln–O6	2.3606(13)	2.3475(13)	2.3351(16)	2.3240(15)	2.3151(12)	2.3082(13)	2.345(2)
Ln–O2	2.3923(13)	2.3740(13)	2.3601(16)	2.3509(15)	2.3443(12)	2.3308(13)	2.372(2)
Average	2.367(15)	2.352(13)	2.339(12)	2.329(13)	2.321(14)	2.311(12)	2.350(13)

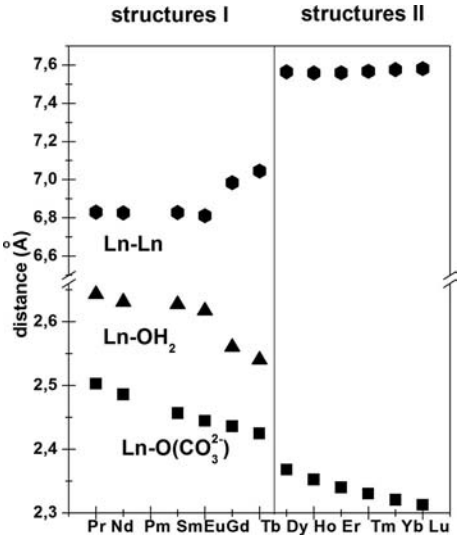

Figure 2. Change in the average bond lengths [Å] for Ln–O(CO_3^{2-}) (■), Ln–O(OH_2) (▲), and Ln–Ln (⬢) distances in **I** and **II**.

plex anion, while in the Gd^{3+} and Tb^{3+} compounds the OW1 molecule is involved in a hydrogen bond with the lattice water molecule, OW2, as shown in Figure 3. For this reason, as well as because of lanthanide contraction, the coordinated water molecule, OW1, is more closely bonded to the Gd^{3+} and Tb^{3+} ions than to the preceding light lanthanide cations.

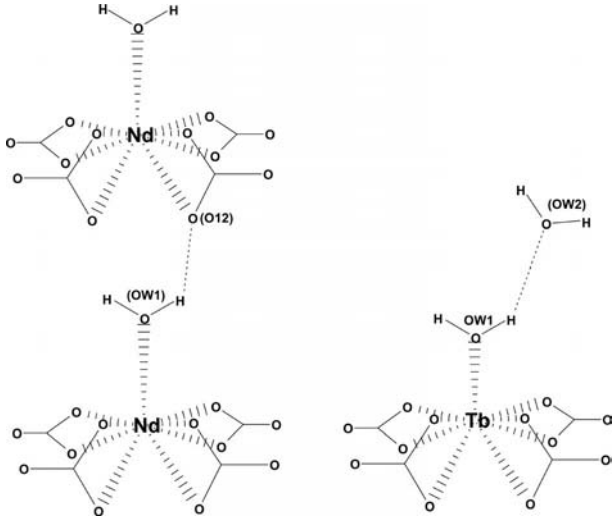

Figure 3. Hydrogen bonds formed by the coordinated OW1 water molecule. The scheme on the left is valid for Pr through Eu and the scheme on the right is valid for Gd and Tb.

In **II**, of the two lattice water molecules, OW2 forms weaker hydrogen bonds than OW1. The change in the Ln–Ln distances also reflects the rearrangement of some of the hydrogen bonds and the drop in the C.N. Interestingly, a slight increase in the Ln–Ln distances was observed in **II** despite the decrease in the cell volume.

The interaction between the Ln^{3+} cation and the CO_3^{2-} anion brought about certain structural changes in the latter. In the $[C(NH_2)_3]_2CO_3$ crystal,[25] all three of the C–O distances, as well as the O–C–O angles, are very similar [1.294(4), 1.294(4), 1.287(5) Å and 120.7(2), 120.7(2), 118.7(4)°, respectively] and the molecular symmetry of the CO_3^{2-} anion is close to D_{3h}.

The theoretically calculated C–O distances for the carbonate anion in vacuo (see the Experimental Section, Theoretical calculations) are 1.319 Å. In the studied crystals, the carbonate anions are deformed, namely, the lengths of the coordinated C–O_c bonds are longer than those of the uncoordinated C–O_u bonds. Moreover, changes in the O–C–O angles were observed. The variation in the average C–O bond lengths and the O–C–O angles for the selected compounds are presented in Table 2.

Table 2. Selected average bond lengths and angles for the uncoordinated and coordinated CO_3^{2-} anions. O_c are the coordinated O atoms; O_u are the uncoordinated O atoms.

	CO_3^{2-} $[C(NH_2)_3]_2CO_3$[25]	$[Pr(CO_3)_4(H_2O)]^{5-}$	$[Lu(CO_3)_4]^{5-}$
	Average bond lengths (Å)		
C–O_c		1.299(14)	1.304(12)
C–O_u	1.292(4)	1.272(6)	1.260(2)
	Average angles (°)		
O_c–C–O_c		117.4(9)	114.8(5)
O_c–C–O_u		121.3(14)	122.6(9)
O_u–C–O_u	120.0(12)		

It is evident that the symmetry of the carbonate anion in the lanthanide tetracarbonates is lower (C_{2v}) than that observed in the $[C(NH_2)_3]_2CO_3$ crystal (D_{3h}). Moreover, it is evident that the heavy lanthanide ions disturb the geometry of the carbonate anion more than the light Ln^{3+} ions because of the lower coordination number and the smaller Ln–O(CO_3^{2-}) distances.

Theoretical Calculations

We thought that it would be interesting to investigate how the change in the charges of the respective atoms, as well as the bond orders, accompanies the geometrical changes in the complex series under discussion. The calculated Bader[26] and Hirshfeld[27] charges, as well as the natural charges,[28] are presented in Table 3. As these quantities do not vary much, we have only shown the values for the closed shell Y, La, and Lu complex anions and for the open shell Dy and Tm complex anions. We have also given the calculated charges for the free (in vacuo) CO_3^{2-} anion for comparison purposes. We have presented only the average values since the difference between the average and the individual atom values did not generally exceed 0.02. Inspection of Table 3 shows that the electric charge migrates towards the central cation. This may be seen if the sum of the O(uncoordinated) and C charges is compared to the sum of the O and C charges in the free carbonate anion. The shift was in the range of 0.05 to 0.07 e in the case of the natural charges, 0.14 to 0.15 e when the Hirshfeld charges were considered (0.18 e was obtained only for the La complex), and 0.08 to 0.09 e for the Bader charges (0.13 e for the La com-

Table 3. The calculated average Bader (Q_B), Hirshfeld (Q_H), and NBO (Q_{NBO}) charges for the selected tetracarbonates of the rare earths together with the free carbonate anion (O_c is the coordinated O atom, O_u is the uncoordinated O atom, Ln is the lanthanide or Y atom). (*) is the charge for the water molecule: O: Q_B = –1.24, Q_H = –0.23, Q_{NBO} = –1.00; H: Q_B = 0.43, Q_H = 0.00, Q_{NBO} = 0.32.

Anion	Ln			O_c			O_u			C		
	Q_B	Q_H	Q_{NBO}	Q_B	Q_H	Q_{NBO}	Q_B	Q_H	Q_{NBO}	Q_B	Q_H	Q_{NBO}
CO_3^{2-}	–	–		–	–		–1.29	–0.65	–0.97	1.88	–0.04	0.90
$[La(CO_3)_4(H_2O)]^{5-(*)}$	2.09	0.17	2.31	–1.20	–0.37	–0.87	–1.33	–0.59	–0.91	2.05	0.08	0.91
$[Y(CO_3)_4]^{5-}$	2.15	0.28	1.84	–1.23	–0.39	–0.85	–1.38	–0.61	–0.93	2.05	0.07	0.91
$[Dy(CO_3)_4]^{5-}$	2.17	0.42	–	–1.23	–0.41	–	–1.37	–0.61	–	2.04	0.06	–
$[Tm(CO_3)_4]^{5-}$	2.05	0.40	–	–1.22	–0.40	–	–1.38	–0.61	–	2.06	0.06	–
$[Lu(CO_3)_4]^{5-}$	2.13	0.29	1.76	–1.23	–0.39	–0.84	–1.37	–0.61	–0.93	2.04	0.07	0.91

plex). The migrated charge, however, does not accumulate on the coordinated oxygen atoms, but partially enters the metal basin. This may be noticed if the charges of the coordinated O atoms are inspected (they have even smaller absolute values than those of the uncoordinated O atoms) on one side and the metal charges are inspected on the other. In the $[Ln(CO_3)_4]^{5-}$ anion series, the transfer is greater at the end of the series (the jump between Tm and Lu may reflect the difference between the open and the closed shell approach). The NBO calculations for the complexes with the closed shell metal cations (Y, La, and Lu; see the Experimental Section) were performed in order to elucidate the nature of the metal–oxygen interaction. In Table 4 we present the calculated Wiberg bond indices in an analogous manner to that presented in Table 3.

Table 4. The Wiberg bond indices. The abbreviations follow those in Table 3, apart from that for OW, which is the water oxygen atom.

Anion	Bond				
	Ln–O_c	C–O_c	C–O_u	Ln–OW	OW–H
$[La(CO_3)_4(H_2O)]^{5-}$	0.14	1.26	1.35	0.05	0.73
$[Y(CO_3)_4]^{5-}$	0.24	1.25	1.34		
$[Lu(CO_3)_4]^{5-}$	0.26	1.25	1.34		
CO_3^{2-}			1.29		

It should be noted that the bond orders for the C–O_u bonds are greater than those for the C–O_c bonds, and also than those for the C–O bonds in the free carbonate anion. On the other hand, the formed Ln–O bonds acquire a certain degree of covalency as the relevant indices show. The covalency is evidently greater in the case of the heavy lanthanides and yttrium than that for the light lanthanides. It is interesting to observe which of the metal orbitals are involved in the covalent interaction with the coordinated oxygen atoms. The calculated natural electron configurations of the metals are as follows: Y – $[Kr]5s^{0.16}4d^{0.90}$, La – $[Xe]4f^{0.24}6s^{0.13}5d^{0.25}$, Lu – $[Xe]4f^{14}6s^{0.19}5d^{0.95}$. In the following discussion we will limit ourselves to the case of Lu where these effects are the most pronounced. The examination of the NBO results revealed that the oxygen hybrids of the approximate composition $sp^{3.7}$ form strongly polarized bonds with the $6s6p5d^4$ (more exactly, $6s6p^{0.8}5d^{4.1}$ on the average) hybrids of lutetium (the superscripts indicate the proportions of the relevant natural atomic orbitals, which form the relevant hybrids). These bonds are, as expected, strongly polarized (approximately 90%); however, owing to their partial covalent character, the metal cations gain additional negative charge. In a more intuitive way, the covalent interactions may be visualized by plotting the canonical DFT orbitals with non-negligible participation of the lanthanide orbitals; such an exemplary drawing for $[Lu(CO_3)_4]^{5-}$ is presented in Figure 4.

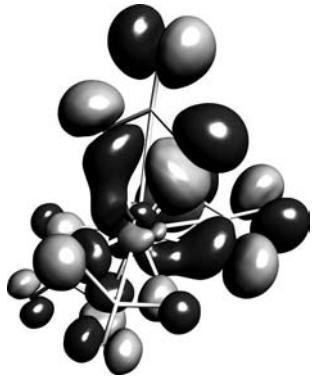

Figure 4. A view of a DFT canonical orbital where mixing of the lone pairs of the O atoms and the Lu orbitals may be observed. The orbital composition is 86.34% p(O), 5.12% f(Lu), and 3.38% d(Lu).

IR Spectroscopy

IR Spectra of the Crystalline Lanthanide Carbonates

The IR spectra of all of the studied rare earth tetracarbonates, as well as $[C(NH_2)_3]_2CO_3$, $[C(NH_2)_3]Cl$, and Na_2CO_3, were recorded in the range of 50 to 4000 cm^{-1} at room temperature. The assignment of the appropriate internal modes of the carbonate anion in Na_2CO_3 and in the studied compounds, following Fujita et al.,[29] together with the wavenumbers are presented in Figure 5, whereas the selected IR spectra of the studied crystals are presented in Figures 6 and 7.

The changes in the nearest surrounding of the Ln^{3+} ion are reflected in the variation of the bands that were observed in the spectral range of 220 to 320 cm^{-1} (Figure 6).

As shown by Fujita et al.[29] for the $[Co(NH_3)_4CO_3]^+$ and $[Co(NH_3)_5CO_3]^+$ complexes, the ν_{M-O} stretching vibration was split in the case of the bidentate CO_3^{2-} coordination mode {$[Co(NH_3)_4CO_3]^+$ – C_{2v} symmetry}, while a single band was observed in the monodendate coordination mode {$[Co(NH_3)_5CO_3]^+$ – C_s symmetry}.

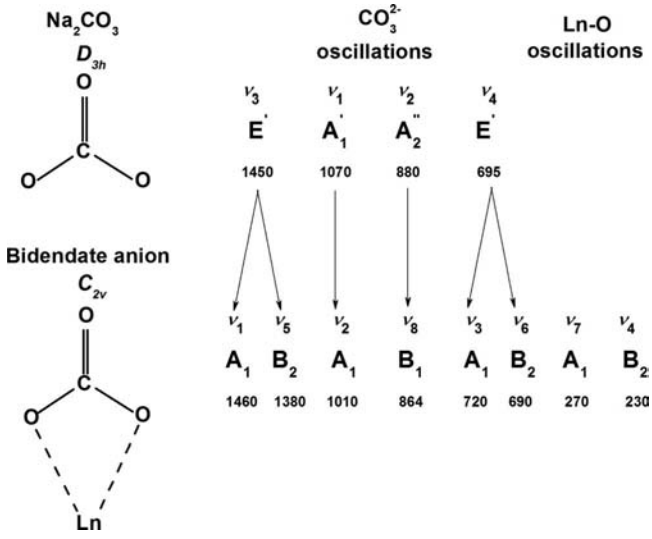

Figure 5. The internal modes of the free and the coordinated CO_3^{2-} anion, together with the wavenumbers [cm^{-1}]. For the uncoordinated CO_3^{2-} the vibrations are labelled as ν_1 for the symmetrical CO stretching, ν_2 for the out-of-plane bending deformation, ν_3 for the doubly degenerate asymmetric CO stretching, and ν_4 for the doubly degenerate in-plane bending.

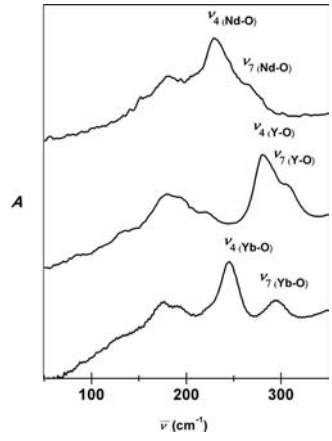

Figure 6. Selected IR spectra of the Nd (**I**) and Y and Yb (**II**) tetracarbonates.

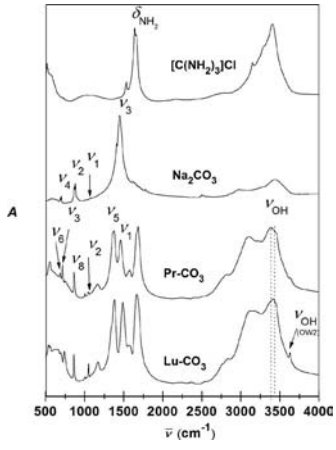

Figure 7. Selected IR spectra of $[C(NH_2)_3]Cl$, Na_2CO_3, $[C(NH_2)]_3[Pr(CO_3)_4(H_2O)]\cdot 2H_2O$, and $[C(NH_2)_3][Lu(CO_3)_4]\cdot 2H_2O$ crystals.

In the studied crystals, the splitting of the ν_{Ln-O} band confirmed the bidentate coordination mode of the carbonate anions. Interestingly, the splitting of the ν_{Ln-O} band ($\Delta_1 = \nu_7 - \nu_4$) was larger in **II** (ca. 50 cm^{-1}) than it was in **I** (ca. 35 cm^{-1}), as shown in Figure 8a.

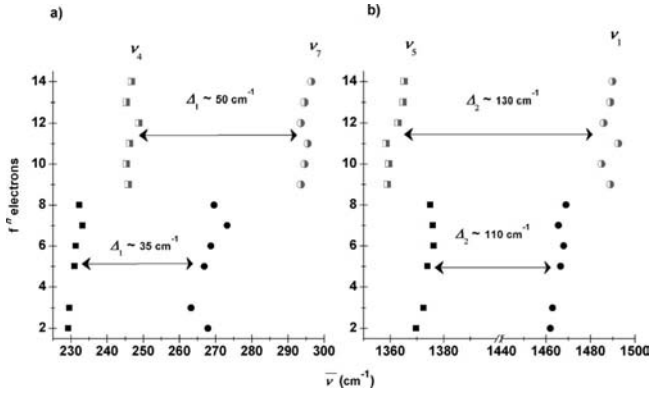

Figure 8. The relationship between the f-electron number and the wavenumbers for (a) ν_{Ln-O} (ν_4 and ν_7); and (b) ν_{C-O}(ν_5 and ν_1) in **I** and **II**.

Both the ν_7 and the ν_4 bands are red-shifted when the Ln–O distances and the coordination number of the Ln^{3+} ions increase. The smaller Δ_1 value (36 cm^{-1}) for Y^{3+} (Figure 6) than for the other lanthanide carbonates in series **II** is caused by the smaller mass of the Y^{3+} ion. This unequivocally confirmed that the bands located between 220 and 320 cm^{-1} (ν_4 and ν_7) may be attributed to the ν_{Ln-O} vibrations.

The second group of bands, which provided valuable information about the Ln–CO_3^{2-} interaction, is located between 1230 and 1550 cm^{-1} and was assigned to the ν_{CO} vibrations. The decrease in the ionic radius and the coordination number of the Ln^{3+} ions, as well as the shortening of the Ln–O(CO_3^{2-}) bond lengths, brought about the ν_5 and ν_1 shift to higher energies. The splitting of the ν_{CO} band ($\Delta_2 = \nu_1 - \nu_5$) is larger in **II** than in **I**, as was the case for the splitting of the ν_{Ln-O} band (Δ_1) (Figure 8). The Δ_2 splitting indicated that the carbonate anion coordinates to Ln^{3+} in a bidentate mode because the value for the monodendate mode is about 50 to 60 cm^{-1}.[29]

The force constants of the ν_{CO_c} and ν_{CO_u} stretching vibrations were determined based on the structural data and the following empirical relation (1):[30]

$$f_{C-O} = \frac{35.5}{r_{CO}^{5.79}} \quad (1)$$

(where f_{C-O} is the force constant, r_{CO} is the C–O bond length), and are compared in Figure 9.

Since the relationship between the f electron number and the f_{C-O} is similar to that shown in Figure 8b, the ν_1 and ν_5 bands may be attributed to the ν_{CO_u} and ν_{CO_c} oscillations, respectively.

The larger splitting of the ν_{LnO} and ν_{CO} bands in **II** than in **I** (Figures 6, 7 and 8) may suggest a higher covalent contribution to the Ln–O bonds in **II** than in **I** and/or a greater rearrangement of the charge distribution in the CO_3^{2-}

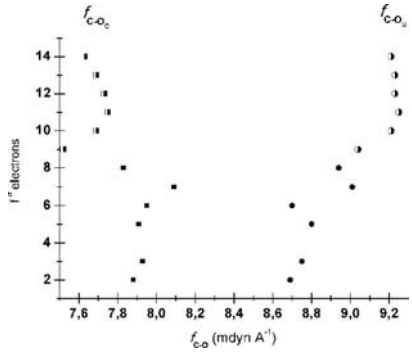

Figure 9. The relationship between the f-electron number and the force constants of the ν_{C-O} stretching vibrations.

anion, as was shown in the theoretical calculations. Moreover, the Δ_2 values, as well as the position of the ν_1 and ν_5 bands, may reflect the change in the coordination number of the Ln^{3+} ions in the studied compounds.

The strong and sharp bands that were found in the region of 1640 to 1720 cm^{-1} were assigned to the δ_{NH_2} and δ_{OH_2} vibrations. The most intense, wide bands that were located in the spectral range between 2500 and 3750 cm^{-1} were attributed to the ν_{NH} and ν_{OH} oscillations and to the $2\nu_{CO}$, $2\delta_{NH_2}$, and $2\delta_{OH_2}$ overtones.[31] A difference in the ν_{OH} positions was observed for **I** and **II**. The broadening of the ν_{OH} band at approximately 3380 cm^{-1} for **I**, in comparison with that at approximately 3420 cm^{-1} for **II**, is consistent with the presence of a coordinated water molecule. It is worth noting that in **II** one of the lattice water molecules, OW2, is involved in weaker hydrogen bonding than OW1. For this reason, the sharp, relatively weak band that was observed at approximately 3630 cm^{-1} may be assigned to the ν_{OH} vibrations of OW2.

IR Spectra of the Lanthanide Carbonates in Solution

The IR spectra of the lanthanide carbonate solutions were measured in the spectral range of 1000 to 4000 cm^{-1}. The bands of the ν_{CO} (1300–1550 cm^{-1}) and δ_{OH} (1600–1750 cm^{-1}) vibrations in the Nd^{3+} and Dy^{3+} complexes in solution spectra, as well as those of H_2O and K_2CO_3, are shown in Figure 10. The spectra of the appropriate Nd^{3+} and Dy^{3+} crystals have been included for comparison purposes.

The peak at 1393 cm^{-1} in the spectra of the Nd^{3+}, Dy^{3+}, and K_2CO_3 solutions was attributed to the uncomplexed carbonate anion. This band partially obscures the bands at 1373 cm^{-1} (ν_5) and 1462 cm^{-1} (ν_1) from the coordinated carbonate anions in the Nd^{3+} complex. Better resolved spectra were observed in the case of the Dy^{3+} carbonate complexes in solution. The shoulder at 1462 cm^{-1} and the peak at 1485 cm^{-1} that were observed in the spectra of the Nd^{3+} and Dy^{3+} solutions, respectively, are assigned to the ν_{CO} vibrations of the uncoordinated C–O bonds from the complexed CO_3^{2-} anion. As previously shown, the difference between the ν_1 band positions in the spectra of **I** (ca. 1460 cm^{-1}) and **II** (ca. 1490 cm^{-1}) may be an indication of the change in the coordination number. The similar values for the ν_1 band maxima in the respective spectra for the **II** crystals and solutions (lower arrow in Figure 10) may suggest that the geometry of the complexes and the coordi-

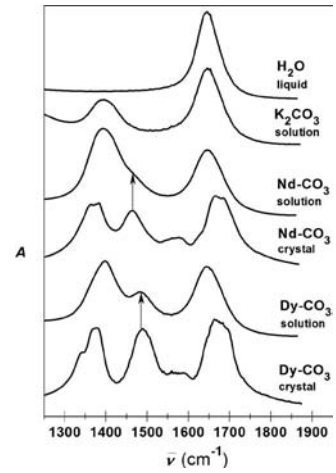

Figure 10. IR spectra of H_2O, K_2CO_3, Nd–CO_3, Dy–CO_3 solutions and the Nd–CO_3, Dy–CO_3 crystals.

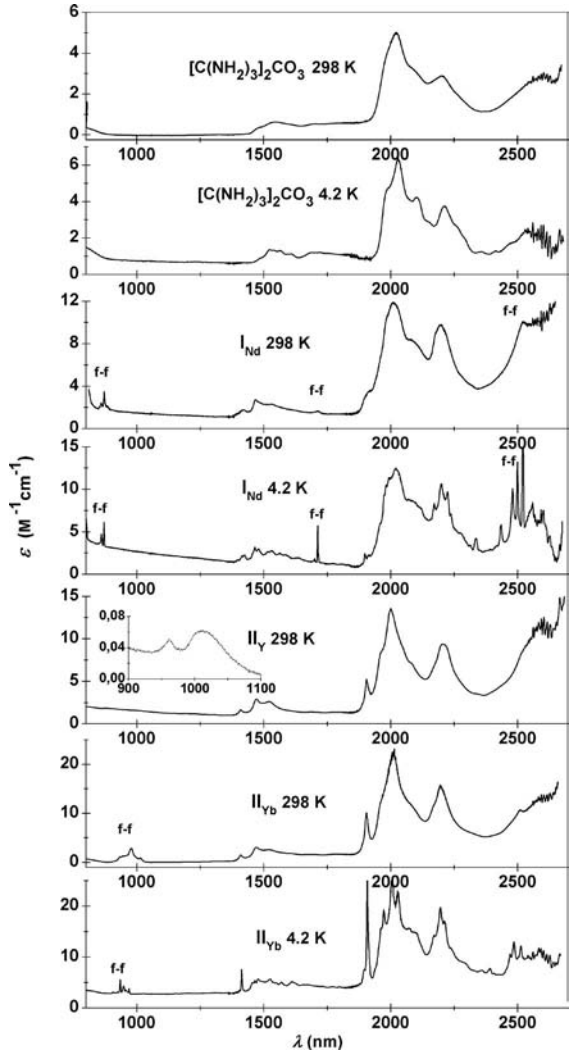

Figure 11. NIR absorption spectra of selected monocrystals at 298 K and 4.2 K.

nation number of the heavy Ln^{3+} ions (8) are similar in both phases. Because the resolution of the light lanthanide spectra was worse, it is difficult to draw similar conclusions about the composition of the metal first coordination sphere for these systems.

NIR Spectroscopy

The analysis of NIR spectra provides important information about possible luminescence deactivation pathways of the f–f transitions. The presence of overtones in this region indicates an increased probability of nonradiative luminescence quenching.

The f–f transition bands of some of the lanthanide ions (e.g. Nd^{3+}, Sm^{3+}, Dy^{3+}, Yb^{3+}) appear between 800 and 3000 nm. In many cases they have an intensity that is comparable to those of the overtone bands. Therefore, to interpret the spectra in this region, knowledge of the ν_{OH}, ν_{NH}, δ_{NH_2}, δ_{OH_2}, and ν_{CO} vibrations is necessary. The wavenumber of the combination bands is close to the sum of the fundamental vibrations and the wavenumber of the overtones, which one may find from Equation (2):

$$\bar{\nu}_{n+1} - \bar{\nu}_n = \varpi\cdot[1 - 2\cdot\chi_{anh}(n + 1)] \quad (2)$$

where $\bar{\nu}_{n+1}$ and $\bar{\nu}_n$ are the wavenumber of the overtone transitions, ϖ is the oscillation constant, and χ_{anh} is the anharmonicity constant.

According to Equation (2), the difference, $\Delta\tilde{\nu}$, should be a linear function of n. This was one of the criteria that was used to identify the respective overtones.

The NIR absorption spectra of the studied crystals were measured at room and liquid helium temperatures and some of them are presented in Figure 11. The characteristic sharp peaks were clearly observed in the Y^{3+} and Yb^{3+} complex spectra at approximately 2100, 1900, 1470, and 1410 nm and were interpreted as the combination bands for $\nu_{5(CO)} + \nu_{OH(OW2)}$, $\nu_{OH(OW1)} + \delta_{NH}$, $\nu_{OH(OW1)} + \nu_{NH}$, and $2\nu_{OH(OW2)}$, respectively. These bands are particularly clear in the spectra of **II**, in which the OW2 water molecule forms a weak hydrogen bond. The assignment of selected bands for the $[C(NH_2)_3]_5[Y(CO_3)_4]\cdot 2H_2O$ crystal are presented in Table 5.

Table 5. Assignement of selected bands in the NIR spectrum of $[C(NH_2)_3]_5[Y(CO_3)_4]\cdot 2H_2O$.

$[C(NH_2)_3]_5[Y(CO_3)_4]\cdot 2H_2O$	$\bar{\nu}$ (cm^{-1})	λ (nm)
$3\nu_{5(CO)}$	3980	2513
$3\nu_{1(CO)}$	4024	2485
$\nu_{5(CO)} + \nu_{NH}$	4522	2211
$\delta_{OH} + \nu_{OH(OW2)}$	4594	2177
$\nu_{1(CO)} + \nu_{NH}$	4594	2177
$3\delta_{NH}$	4753	2104
$\nu_{5(CO)} + \nu_{OH(OW2)}$	4813	2078
$4\nu_{5(CO)}$	4990	2004
$\nu_{5(CO)} + \nu_{OH(OW1)}$	5000	2000
$4\nu_{1(CO)}$	5070	1972
$\nu_{OH(OW1)} + \delta_{NH}$ and/or $2(\nu_{1(CO)} + \nu_{5(CO)})$	5252	1904
$\nu_{OH(OW2)}+\nu_{NH}$	6575	1521
$\nu_{OH(OW1)}+\nu_{NH}$	6798	1471
$2\nu_{OH(OW2)}$	6798	1471
$2\nu_{OH(OW1)}$	7091	1408
$3\nu_{OH(OW1)}$	9872	1013
$3\nu_{OH(OW2)}$	10403	961

UV/Vis Spectroscopy

Reflectance Spectra

The UV/Vis reflectance spectra of the lanthanide carbonates were measured at room temperature (Figure S1). Weak intramolecuar n→π* transition of the carbonate anion may be observed in the spectral range of 200 to 250 nm.[32] It should be noted that the n→π* transition is hypsochromically shifted in the spectra of **I** and **II** in relation to that observed in the spectra of Na_2CO_3 and $[C(NH_2)_3]_2CO_3$. The energy of the n→π* transition increased with the number of f^n electrons in the series of lanthanide complexes (Table 6).

Table 6. The n→π* transition wavenumber in the crystal spectra.

Crystal	n→π* (cm^{-1})
$[C(NH_2)_3]_2CO_3$	42480
Na_2CO_3	43480
$[C(NH_2)_3]_5[Nd(CO_3)_4(H_2O)]\cdot 2H_2O$	43690
$[C(NH_2)_3]_5[Dy(CO_3)_4]\cdot 2H_2O$	43760
$[C(NH_2)_3]_5[Tm(CO_3)_4]\cdot 2H_2O$	43810
$[C(NH_2)_3]_5[Lu(CO_3)_4]\cdot 2H_2O$	44270

These data may suggest that the electron lone pairs of the carbonate oxygen atoms are affected by the metal–ligand bond formation and the concomitant electron density transfer from the carbonate oxygen atoms into the empty 6s and 5d orbitals of the Ln^{3+} ion, as was shown from the theoretical calculations. This leads to a lowering of the energy of the non-bonding orbitals and, consequently, to a hypsochromic shift of the n→π* transition results.

Absorption Spectra of the f–f Transitions

The absorption spectra of some of the f–f bands of the lanthanide carbonates are presented in Figures 12 (monocrystals) and S2 (aqueous solutions). The oscillator strengths of the f–f transitions and the Judd–Ofelt, Ω_λ,[33,34] parameters [Equation (11) in the Experimental Section] for the Pr^{3+}, Nd^{3+}, Sm^{3+}, Eu^{3+}, Dy^{3+}, Ho^{3+}, Er^{3+}, and Tm^{3+} compounds in both phases were determined and are given in Table 7 and S3.

The lanthanide ions Nd^{3+}, Ho^{3+}, and Er^{3+} were the most suitable for the f–f transition intensity analysis because their hypersensitive bands are not disturbed by the electronic transitions of the ligand in UV or by overtones in the NIR region. In the case of Pr^{3+}, Sm^{3+}, Dy^{3+}, and Tm^{3+}, the hypersensitive transition bands often coalesce with the first overtone of water ($2\nu_{OH}$). For this reason the inclusion of these bands in the fitting of the Ω_λ parameters can yield biased results, as has been shown by Mondry and Bukietyńska.[35]

Significant differences between the Ω_λ values for both of the phases (crystals and solutions) were observed for the Nd^{3+} complexes whereas, for the Er^{3+} compounds, the Ω_λ

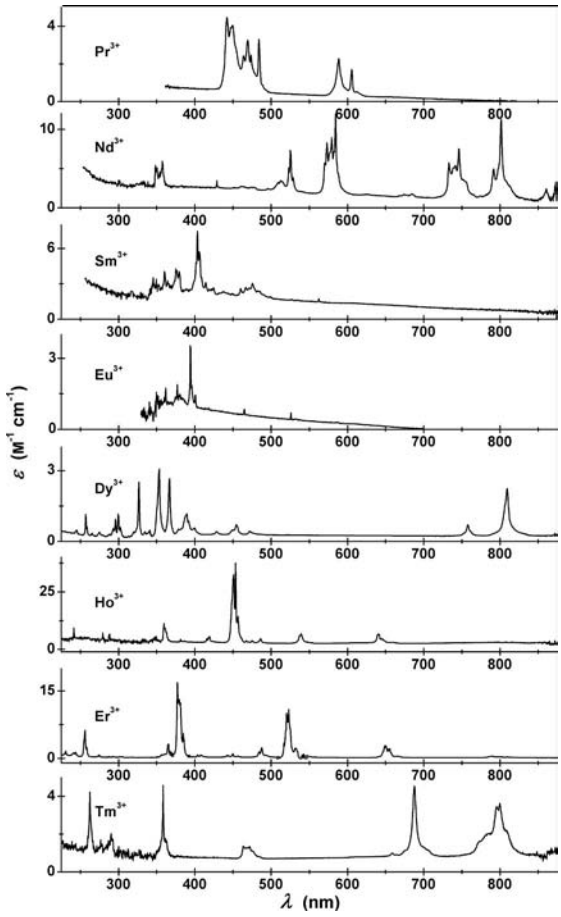

Figure 12. The absorption spectra of the Ln–carbonate crystals.

parameters are similar for both of the phases. This suggests that for Nd^{3+} the coordination sphere of the metal ion in solution is different from that in the crystal, while in the case of heavy lanthanides the nearest surrounding of the metal ion is rather similar in both of the phases.

From among the Ω_λ parameters, Ω_2 is the most sensitive to the polarizability of the coordinated ligands,[36] as well as the covalent[24] and vibronic effects,[37] while Ω_4 and Ω_6 are more dependent on the crystal field and the covalent interactions.[38] Mason and Taranter[36a] calculated the contribution of ligand polarizability and the crystal field effect to the total values of the Ω_λ(tot) parameters for eight-coordinate lanthanide(III) tetrakis(dithiocarbamate). The authors concluded that the ligand polarizability contribution to Ω_λ(tot) decreases from 66% to 17% and 0.1% for λ = 2, 4, 6, while the corresponding contribution of the crystal field increases from 5% to 57% and 98.5%. The changes in the Ω_λ parameters for all of the studied compounds in the crystal phase and in solution are presented in Figure 13. The variation in the Ω_2 and Ω_4 parameters is irregular, which may confirm that many factors, which are acting in opposite directions, affect them. However, a clear trend in the changes of Ω_6 was observed, namely, that Ω_6 decreased with the increasing atomic number for the Ln^{3+} ion. These changes may be rationalized in terms of greater rigidity of the carbonate systems[39] and/or increased covalent effects. Due to the increased influx of electron density in the 6s orbitals, which leads to the screening and the contraction of the 5d shell, the reduction in the $\langle 4f|r^n|5d\rangle$ radial integrals (to which the Ω_6 parameter is particularly sensitive) takes place.[40] This explanation is consistent with the results of the DFT calculations (presented above), which indicated that the transfer of the charge density onto the metal ion orbitals is stimulated more efficiently by the carbonate anion than by the water molecule.

Analysis of Selected f–f Transitions

Hypersensitive Transitions

The hypersensitive f–f transitions are those that are strongly influenced by the changes in the nearest surrounding of the Ln^{3+} cation. Thus, the analysis of these transitions may provide valuable information on the coordination chemistry of the lanthanide ions. The experimental data indicated that the intensity of the hypersensitive transitions mainly depends on the symmetry of the lanthanide complex, the polarizability of the ligands,[41] and the covalency degree of the Ln–L bond.[24] Generally, the binding of soft polarizable ligands brings about an increase in the hypersensitive transition intensities.[42] The hypersensitive transition spectra of the Nd^{3+} and Er^{3+} carbonate complexes in solution and in the crystal phase are presented in Figure 14.

There are significant differences in the intensities, shapes, and positions of the peak maxima in the Nd complex spectra, whereas the Er spectra are more similar to each other.

In order to assess the effect of the carbonate ion coordination in solution, the ratios of the hypersensitive transition intensities in solution and in crystal (hereinafter $P_{solution}/P_{crystal}$) were compared (Figure 15).

These ratios are greater than 1 for the light lanthanides and very close to 1 for the heavy Ln^{3+} ions. In the case of Pr^{3+} and Tm^{3+}, however, the hypersensitive transitions ($^3H_4\rightarrow{}^3F_2$ and $^3H_6\rightarrow{}^3F_4$, respectively) coalesce with the overtones and the combination bands of the OH and NH group vibrations and, therefore, the pseudo-hypersensitive transitions $^3H_4\rightarrow{}^3P_2$ of Pr^{3+} and $^3H_6\rightarrow{}^3H_4$ of Tm^{3+} were taken into consideration. Likewise, the hypersensitive transition of Dy^{3+} ($^6H_{15/2}\rightarrow{}^6H_{9/2}$, $^6F_{11/2}$) coincides with the $2\nu_{OH}$ overtone, therefore the NIR absorption spectra of the solution was recorded with reference to a solution of the analogous yttrium complex. The $^2F_{7/2}\rightarrow{}^2F_{5/2}$ transition of Yb^{3+} is not a typical hypersensitive transition because $\Delta J \neq 2$.

In order to explain the large $P_{solution}/P_{crystal}$ value observed for the Eu^{3+} carbonates, it should be noted that all of the considered hypersensitive transitions, except for that of Eu^{3+}, have non-zero $U^{(4)}$ and/or $U^{(6)}$ matrix elements. Thus, the influence of the ligand polarizability on the oscillator strength, which is manifested the most through the value of the Ω_2 parameter, is tempered by the part dependent on $U^{(4)}$ and/or $U^{(6)}$ [see Equation (11)]. However, in the case of Eu^{3+}, $U^{(4)}$ and $U^{(6)}$ are equal to 0 for the hypersensitive $^7F_0\rightarrow{}^5D_2$ transition. It should be noted that the observed oscillator strength of this transition in solution (P =

Table 7. The oscillator strengths (P·10^8) and Ω_λ parameters for the Ln^{3+} –CO_3^{2-} complexes in single crystals and in solutions ($c_{Ln^{3+}}$ = 0.050 M, $c_{K_2CO_3}$ = 2.4 M, pH ≈ 12 at 298 K). The hypersensitive transitions are printed in bold.

Nd	Crystal	Solution	Ho	Crystal	Solution	Er	Crystal	Solution
$^4I_{9/2} \rightarrow$			$^5I_8 \rightarrow$			$^4I_{15/2} \rightarrow$		
$^2L_{17/2}$, $^4D_{7/2}$, $^2I_{13/2}$		212.21	$(^3F,^5D)_3$	365.62	231.17	$^2I_{13/2}$, $(^2P,^2D)_{3/2}$	137.17	
$^2L_{15/2}$,$^4D_{1/2}$,$^2I_{11/2}$, $^4D_{5/2}$,$^4D_{3/2}$	575.54	1161.05	$^3I_6$, $(^3D,^5D,^3P)_1$, $^5D_1$		68.27	$^2I_{11/2}$, $^2L_{17/2}$, $^4D_{3/2}$	279.11	
$^2D_{5/2}$	3.64	6.47	$(^3P,^1D)_2$, $^3L_7$, $^3I_7$, $^3F_4$, $^3I_5$, $^3M_9$		120.32	$^2D_{5/2}$, $^4D_{7/2}$	1091.06	1252.14
$^2P_{1/2}$	34.87	42.93	$^3P_0$, $(^3H,^5D,^1G)_4$, $^3F_2$, $^1L_8$, $(^3H,^3G)_5$	247.03	328.18	$(^2H,^2G)_{9/2}$	71.97	71.18
$^2K_{15/2}$, $^2G_{9/2}$, $(^2D,^2F)_{3/2}$, $^4G_{11/2}$	144.37	188.10	$(^5G,^5D^3G)_4$, $(^3F,^3G)_3$	285.69	317.61	$^2D_{5/2}$	9.10	7.92
$^4G_{9/2}$,$^4G_{7/2}$,$^2K_{13/2}$	726.03	1203.15	$^3M_{10}$, $^3L_8$	77.70	154.23	$^4G_{7/2}$	14.10	19.16
$^2G_{7/2}$,$^4G_{5/2}$	**1693.69**	**4013.26**	$(^3F,^3H^3G)_4$, $^3K_6$	139.59	90.12	$^2K_{13/2}$, $^4G_{5/2}$, $^2P_{1/2}$	28.27	28.05
$^2H_{11/2}$	11.87	19.47	$^5G_3$, $^3L_9$	89.77	177.38	$(^2P,^2D,^4F)_{3/2}$	9.86	8.78
$^4F_{9/2}$	51.19	71.33	$(^5G,^3H)_5$, $^3H_6$, $(^5F,^3F,^5G)_2$	1116.62	1325.53	$^4G_{9/2}$, $^2K_{15/2}$, $^4G_{9/2}$	235.44	430.69
$^4F_{7/2}$,$^4S_{3/2}$	743.34	950.22	$^5G_4$, $^3K_7$	104.69	139.87	$^4G_{11/2}$	**2992.28**	**2914.65**
$^4F_{5/2}$,$^2H_{9/2}$	734.31	896.48	$(^5G,^3G)_5$	334.23	363.93	$(^2G,^4F,^2H)_{9/2}$	82.07	86.68
$^4F_{3/2}$	127.93	209.33	$^5G_6$, $^5F_1$	**4566.32**	**5267.01**	$^4F_{5/2}$, $^4F_{3/2}$	105.52	99.93
			$^5F_2$, $^3K_8$	77.37	170.93	$^4F_{7/2}$	239.00	221.53
			$^5F_3$	140.74	168.00	$^2H_{11/2}$	**1449.78**	**1519.32**
			$^5S_2$, $^5F_4$	440.00	447.69	$^4S_{3/2}$	38.37	69.30
			$^5F_5$	364.58	343.78	$^4F_{9/2}$	273.96	243.90
			$^5I_5$	32.74	28.33	$^4I_{9/2}$	43.05	39.72
			$^5I_6$	113.23	105.31	$^4I_{11/2}$	90.85	90.40
Ω_2·10^{20} (cm^2)	5.31 ± 0.54	14.68 ± 0.22		13.88 ± 0.30	17.99 ± 0.35		11.00 ± 0.30	11.76 ± 0.22
Ω_2·10^{20} (cm^2)	2.16 ± 0.49	5.07 ± 0.20		3.29 ± 0.35	3.53 ± 0.42		3.36 ± 0.22	4.02 ± 0.16
Ω_2·10^{20} (cm^2)	6.23 ± 0.69	8.31 ± 0.28		2.09 ± 0.35	2.60 ± 0.41		1.26 ± 0.39	1.11 ± 0.30
rms·10^7	11.0	15.4		6.82	7.33		6.95	4.65

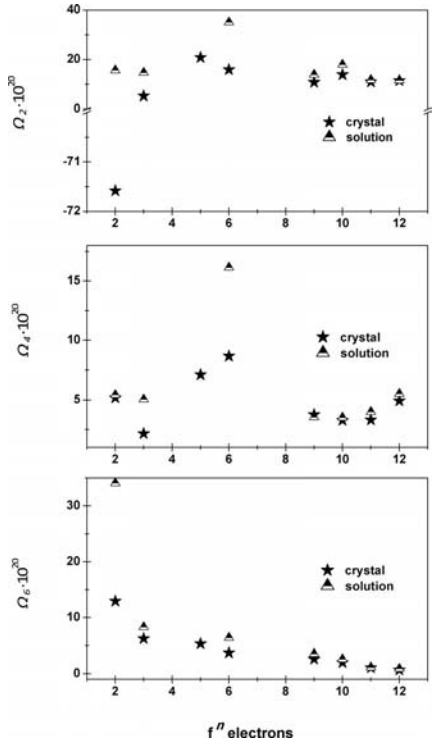

Figure 13. The Ω_λ parameter changes for the lanthanide carbonates in solution and in the crystal phase.

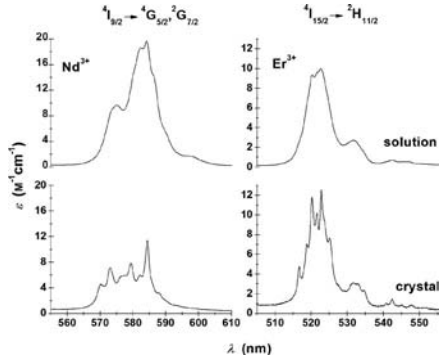

Figure 14. The hypersensitive transitions of the Nd^{3+} (left) and Er^{3+} (right) carbonate complexes as crystals (bottom) and in solution (top).

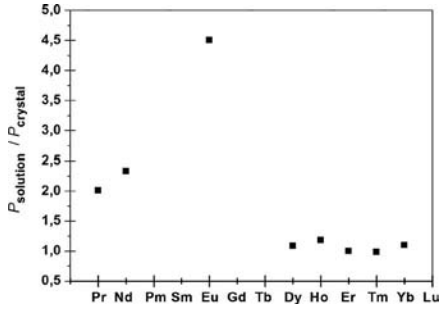

Figure 15. The oscillator strength ratios of selected lanthanide hypersensitive transitions, $P_{solution}/P_{crystal}$, for the lanthanide carbonate complexes in solution and as crystals.

53.94×10^{-8}) is one of the largest reported in the literature.[43]

By taking into account the structural data, as well as the electronic absorption and the IR spectroscopy results, it may be concluded that the coordination environments of the heavy lanthanide ions in the carbonate complexes in solution and in the solid state are similar. Hence, the $[Ln(CO_3)_4]^{5-}$ species appear to predominate. The data presented in Figures 14 and 15 show that the coordination environments for the light lanthanide ions in the crystals and in solution differ. Moreover, the $P_{solution}/P_{crystal}$ ratio may indicate that the surrounding of the light Ln^{3+} ions contains more polarizable components and the overall average allocation of the ligands around the metal cation may be more anisotropic in solution than in the crystals. As far as the polarizability is concerned, it is useful to point out that the experimental values, α, determined for the H_2O molecule in $CaSO_4 \cdot 2H_2O$ (gypsum)[44] and for the CO_3^{2-} anion in $CaCO_3$ (calcite)[45] are 1.442 Å^3 and 3.85 Å^3, respectively.

$^4I_{9/2} \rightarrow {}^2P_{1/2}$ and $^7F_0 \rightarrow {}^5D_0$ Transitions

Valuable information about equilibria in solution may be provided by the analysis of the $^4I_{9/2} \rightarrow {}^2P_{1/2}$ transition for the Nd^{3+} compounds and the $^7F_0 \rightarrow {}^5D_0$ transition for the Eu^{3+} complexes. The $^4I_{9/2} \rightarrow {}^2P_{1/2}$ transition reveals splitting of the ground level of Nd^{3+} in the ligand field, while the number of components observed in the $^7F_0 \rightarrow {}^5D_0$ transition renders directly the number of chemically distinct environments of the Eu^{3+} ion. The position of the $^4I_{9/2} \rightarrow {}^2P_{1/2}$ and $^7F_0 \rightarrow {}^5D_0$ transitions may be an indicator of the nephelauxetic effect, which is connected with the metal–ligand distances, the coordination numbers, and the total negative charge accumulated around the metal cation.[46] The spectra of the $^4I_{9/2} \rightarrow {}^2P_{1/2}$ and $^7F_0 \rightarrow {}^5D_0$ bands in solution and in the single crystals at 300 K and 4.2 K are presented in Figure 16.

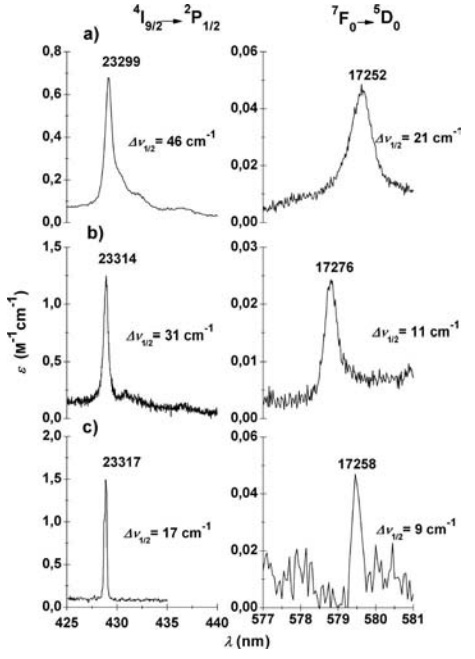

Figure 16. The spectra of the $^4I_{9/2} \rightarrow {}^2P_{1/2}$ and $^7F_0 \rightarrow {}^5D_0$ transitions for the Nd^{3+} and Eu^{3+} complexes (a) in solution ($c_{Ln^{3+}}$ = 0.050 M, $c_{CO_3^{2-}}$ = 2.4 M) and in crystals (b) at 300 K and (c) at 4.2 K ($c_{Nd^{3+}}$ = 2.39 M, $c_{Eu^{3+}}$ = 2.43 M).

In both cases, the band maxima in the solution spectra are batochromically shifted in comparison to those in the crystal spectra. Significant differences in the $^4I_{9/2} \rightarrow {}^2P_{1/2}$ and $^7F_0 \rightarrow {}^5D_0$ peak positions in the respective spectra for the solutions and the crystals confirmed that the coordination environments of the light lanthanide ions in both of the phases are different. Moreover, the larger half widths ($\Delta\nu_{1/2}$) of the appropriate transitions in solution indicated an equilibrium between the different species. In the low temperature spectra (4.2 K) of the Nd^{3+} crystal, the $^4I_{9/2} \rightarrow {}^2P_{1/2}$ band is slightly shifted in comparison to that at 298 K, while in the case of Eu^{3+}, the $^7F_0 \rightarrow {}^5D_0$ band is significantly shifted (18 cm^{-1}) to a lower energy at 4.2 K. Moreover, the $^7F_0 \rightarrow {}^5D_0$ band in the studied Eu^{3+} crystal at 4.2 K is hypsochromically shifted to 17258 cm^{-1} in comparison with the band that was observed in the $Na_3[Eu(CO_3)_3]$ crystal at 9 K (17234 cm^{-1}).[12]

Luminescence Spectroscopy

Luminescence Lifetimes

The luminescence lifetimes of Eu^{3+}, Tb^{3+} and Dy^{3+} carbonate complexes in solution and in crystals were determined and are compared in Table 8. The average number of coordinated water molecules was also evaluated in two ways by using Equations (3) and (4):

$$q_{Ln} = A \cdot \left(\frac{1}{\tau_{H_2O}} - \frac{1}{\tau_{D_2O}}\right)\text{[47]} \quad (3)$$

$$q'_{Ln} = A' \cdot \left(\frac{1}{\tau_{H_2O}}\right) - B\text{[48]} \quad (4)$$

where A = 1.05 for Eu^{3+} and 4.2 for Tb^{3+}; A' = 1.1 and B = 0.71 for Eu^{3+}; A' = 4.0 and B = 1.0 for Tb^{3+}; A' = 0.024 and B = 1.3 for Dy^{3+}; A, A', and B are in milliseconds.

Table 8. The luminescence lifetimes and the calculated number of coordinated water molecules for the Eu, Tb and Dy carbonate complexes in solution. The precision of the presented luminescence lifetimes is ±10% and q ± 0.5.

	Crystal	Solution		Crystal	Solution	
	τ (μs)	τ_{H_2O} (μs)	τ_{D_2O} (μs)	q'_{H_2O}	q_{H_2O}	q'_{H_2O}
Eu	625	455	1260	1.0	1.5	1.7
Tb	1920	1240	1290	1.1	0.1	2.2
Dy	10.5	10.0	85	1.0		1.1

The determined q_{H_2O} values for the respective lanthanide complexes significantly differ and depend on which of the equations (3 or 4) was used in the calculations. The estimation of the number of coordinated water molecules, which was accurate in the case of the Eu and Tb crystals, completely failed in the case of Dy. On the other hand, the measured lifetimes for the Dy crystal and solution were practically identical, which suggests that the coordination environment composition for Dy^{3+} in both systems is very similar. For Eu, the number of coordinated water molecules

tends to oscillate around 1.5. For the Tb solutions, the q_{H_2O} and q'_{H_2O} values are divergent and, moreover, they are different from that estimated in the crystal. By taking into account the insignificant difference between the Tb^{3+} emission lifetimes in H_2O and D_2O, we were inclined to think that the number of water molecules that are coordinated to the metal cation is actually close to zero.

Luminescence Quantum Yields

For the Eu^{3+}, Tb^{3+}, and Dy^{3+} compounds, the luminescence quantum yields (Φ) with respect to quinine sulfate, fluoresceine, and/or $[Ru(bpy)_3]Cl_3$ were determined at different concentrations of the complexes. In addition, the quantum yields (Φ_{calc}) of the Eu^{3+} and Dy^{3+} complexes were estimated by using the calculated τ_{rad} according to the relation (5):

$$\Phi_{calc} = \frac{\tau_{exp}}{\tau_{rad}} \quad (5)$$

where τ_{exp} and τ_{rad} are the experimental and radiative luminescence lifetimes, respectively. In order to determine the radiative luminescence lifetimes for the Eu^{3+} complexes, the following Equation (6) was applied:[49]

$$\frac{1}{\tau_{rad}} = A_{MD} \cdot n^3 \cdot \left(\frac{I_{tot}}{I_{MD}}\right) \quad (6)$$

where $A_{MD} = 14.65\ s^{-1}$,[33,34] n is the refractive index, I_{tot} is the sum of the integrated intensity of the $^5D_0 \rightarrow {}^7F_{0,1,2,3,4}$ transitions, and I_{MD} is the integrated intensity of the $^5D_0 \rightarrow {}^7F_1$ transition, which is assumed to be constant and independent of the coordination environment. For the Dy^{3+} complexes, the τ_{rad} values were calculated according to formula (7):[33,34]

$$\frac{1}{\tau_{rad}} = \sum \frac{64\pi^2 e^2 \bar{\nu}^3}{3h(2J+1)} \cdot \frac{n(n^2+2)^2}{9} \cdot \sum_{\lambda} \Omega_\lambda \cdot \left|\left\langle 4f^N \psi J \left\| U^{(\lambda)} \right\| 4f^N \psi' J' \right\rangle\right|^2 \quad (7)$$

where e is the charge of the electron, $\bar{\nu}$ is the wavenumber of the band maximum, h is Planck's constant, $2J + 1$ is the degeneracy of the ground state, n is the refractive index, $\langle f^N \psi J \| U^{(\lambda)} \| f^N \psi' J' \rangle$ are the relevant reduced matrix element of the unit tensor operator $U^{(\lambda)}$, and Ω_λ are determined from absorption spectra [Equation (11)]. The first sum runs over all of the transitions from $^4F_{9/2}$ to the lower lying states. The luminescence quantum yield results for the studied compounds are presented in Table 9.

Interestingly, in the case of the Eu^{3+} complexes, the Φ values (independent from the determination method) are larger in solution than in the crystal, while the Φ values (by taking into account the experimental errors that resulted from the relatively low intensity of the Dy^{3+} luminescence) are similar in both of the phases for Dy^{3+}.

It is well known that the presence of H_2O in the lanthanide first coordination sphere contributes to nonradiative deexcitation of luminescence and, as a consequence, reduces the quantum yield of the lanthanide luminescence.

Table 9. The luminescence quantum yields (%) for the Eu^{3+}, Tb^{3+}, and Dy^{3+} compounds in solution and in the solid state determined relative to quinine sulfate (Φ_Q), fluoresceine (Φ_F), $[Ru(bpy)_3]^{3+}$ (Φ_{Ru}), and Φ_{calc} (the total concentration of CO_3^{2-} was 2.4 M).

c_{Eu} (M)	Φ_F	Φ_{Ru}	Φ_{calc}	c_{Tb} (M)	Φ_F	c_{Dy} (M)	Φ_Q	Φ_F	Φ_{calc}
0.246	24	27	20	0.199	51	0.249	0.9	1.2	
0.114	23	26	19	0.124	53	0.116	1.4	1.9	
0.0571	21	23	18	0.0597	46	0.0580	1.6	2.3	
0.0286	19	21	20	0.0298	48	0.0290	1.8	2.5	
0.0143	16	19	23	0.0149	51	0.0145	2.0	2.7	
0.00571	21	23	28	0.00597	48	0.00580	2.0	2.8	
0.00286	25	29	27	0.00299	47	0.00290	2.0	2.9	
0.00143	25	28	28	0.00179	52				
0.000715	24	27	27	0.000896	59				
Average	22	25	23		50		1.7	2.3	1.2
Crystal			16			Crystal			1.3

Stern–Volmer Quenching Constants

In order to determine if polynuclear complexes are formed in considerable amount, the Stern–Volmer K_{SV} quenching constants, which are defined by Equations (8) and (9):

$$K_{SV}^{\Phi} = \frac{I_{Tb} - I_{Tb,Eu}}{I_{Tb,Eu} \cdot c_{Eu}} \quad (8)$$

$$K_{SV}^{\tau} = \frac{\tau_{Tb} - \tau_{Tb,Eu}}{\tau_{Tb,Eu} \cdot c_{Eu}} \quad (9)$$

were determined. $K_{SV}{}^{\Phi}$ and $K_{SV}{}^{\tau}$ are the Stern–Volmer quenching constants that were determined from the luminescence intensity (I) or the luminescence lifetime (τ), and I_{Tb}, $I_{Tb,Eu}$, I_{Eu}, τ_{Tb}, $\tau_{Tb,Eu}$, τ_{Tb} are the appropriate luminescence quantities in the presence or absence of the quencher (Eu^{3+}). As shown previously,[50] the quenching of the donor luminescence may result from static interactions (polynuclear donor-acceptor complex formation) or from dynamic factors (collisional deactivation). The equality of $K_{SV}{}^{\Phi}$ and $K_{SV}{}^{\tau}$ shows that the quenching is a result of dynamic factors only. The K_{SV} constants for the Tb^{3+}–Eu^{3+}–CO_3^{2-} aqueous solutions were determined and are compared in Table 10.

Table 10. The Stern–Volmer quenching constants.

c_{Tb} (M)	c_{Eu} (M)	I_{Tb}	I_{Tb-Eu}	$K_{SV}{}^{\Phi}$	τ_{Tb} (μs)	τ_{Tb-Eu} (μs)	$K_{SV}{}^{\tau}$
1.49×10^{-2}	–	19.3	–		1240	–	
1.49×10^{-2}	1.43×10^{-4}	19.3	18.2	423	1240	1168	431
1.49×10^{-2}	1.43×10^{-3}	19.3	12.4	389	1240	802	382
1.49×10^{-3}	–	1.96	–		1243	–	
1.49×10^{-3}	1.43×10^{-4}	1.96	1.85	416	1243	1169	443

The similar values of the $K_{SV}{}^{\Phi}$ and $K_{SV}{}^{\tau}$ constants indicated that no significant amount of the polynuclear species was present and that the monomeric species dominates in the terbium carbonate solutions.

Discussion and Conclusions

The structural and spectroscopic properties of the monocrystalline lanthanide carbonates $[C(NH_2)]_3[Ln(CO_3)_4(H_2O)]\cdot 2H_2O$ (where Ln = Pr^{3+}, Nd^{3+}, Sm^{3+}, Eu^{3+}, Gd^{3+}, Tb^{3+}) and $[C(NH_2)]_3[Ln(CO_3)_4]\cdot 2H_2O$ (where Ln = Y^{3+}, Dy^{3+}, Ho^{3+}, Er^{3+}, Tm^{3+}, Yb^{3+}, Lu^{3+}) were determined. All of the compounds are monomeric. In the first series, the metal cation is nine coordinate and is surrounded by 4 bidentate carbonate anions and a water molecule, while in the other series, the metal coordination number is eight and has 4 bidentate carbonate anions. The structural change was observed between Tb^{3+} and Dy^{3+}.

The change in the C.N. and the Ln–O bond lengths and character in the studied crystals were clearly visible in the IR spectra, namely, the splitting of the ν_{LnO} and ν_{CO} bands in the case of the heavy lanthanides are approximately 15 and 20 cm^{-1} larger, respectively, than those in the light lanthanides. These differences may be connected with the decrease in the Ln–O(CO_3^{2-}) distances in the case of **II**. These data may also suggest that the stronger Ln–O interactions in **II** are brought about by the larger impact of covalency in **II** than in **I**. In order to elucidate the nature of the metal–oxygen interaction, the NBO calculations for the closed shell metal cations were performed. Inspection of the NBO results revealed that the oxygen hybrids, which had the approximate composition $sp^{3.7}$, form strongly polarized bonds with the $6s6p5d^4$ hybrids of the lanthanide cation. These bonds are, as expected, strongly polarized (90%). The covalency is evidently greater in the case of the heavy lanthanides and yttrium than for the light lanthanides. This statement, of course, should not be confused with the assessment of the role of the covalent interactions that involve the 4f subshell, where it is commonly agreed that the latter interactions are larger for the light lanthanides.

The comparison between the IR spectra of the studied complexes in solid state with those in aqueous solution suggested that the coordination number of the predominating species in solution for the heavy lanthanides complexes is 8. In the case of the light lanthanides, the splitting of ν_{CO} was smaller and resulted in the ν_1 and ν_5 bands from the Ln–CO_3^{2-} complexes being partially obscured by the intense ν_{CO} from the uncomplexed CO_3^{2-} anion. Thus, a similar comparison for these elements was not possible.

Despite many works devoted to the lanthanide carbonate complexes in aqueous solutions, their structure remains a complex and debatable problem. The thermodynamic stability constants that were obtained from the extraction and potentiometry methods and, particularly, from the solubility studies of $Na[Ln(CO_3)_2]\cdot nH_2O$ indicated that the limiting species is $[Ln(CO_3)_4]^{5-}$ in the concentrated alkali metal carbonates. However, Philippini et al. stated that in the case of the heavy lanthanides (from Eu to Lu), $[Ln(CO_3)_3]^{3-}$ seems to be the limiting complex.[5,8,9]

We decided to investigate the speciation of the carbonates by taking advantage of the analysis of the f–f transitions, which has previously been successfully applied to identify the structure and stoichiometry of various complexes in aqueous solution.[23]

The analysis of the UV/Vis/NIR absorption spectra led to certain conclusions about the stoichiometry of the complexes and the coordination modes of the carbonate anions. The remarkable agreement between the spectral properties (shape of bands, crystal field components, Judd-Ofelt parameters, luminescence lifetimes, and quantum yields) of the heavy lanthanide (from Dy to Yb) carbonate complexes in the monocrystals and in solution unambiguously suggested that the coordination environments of these cations are very similar in both of the phases. This led to the conclusion that $[Ln(CO_3)_4]^{5-}$ is the predominant form (in the case of the heavy lanthanides) in the concentrated potassium carbonate solutions.

The analysis of the spectral properties of the light lanthanide carbonate complexes was not as straightforward. Although the crystal structures suggested that the $[Ln(CO_3)_4(H_2O)]^{5-}$ species was a good candidate to exist in solution, the spectroscopic data for these complexes in both of the phases were remarkably different. Firstly, a significant increase in the intensities of the hypersensitive transitions, as well as the Judd–Ofelt parameter values, was observed in solution compared to those observed for the relevant crystals. These increases may indicate that the symmetry of the complexes in solution is lower than that in the crystal and/or that the first coordination sphere of Ln^{3+} is filled to a greater degree with strongly interacting ligands, namely, polarizable CO_3^{2-} and/or OH^-. The ligand polarizabilities increase as follows $\alpha_{H_2O} = 1.442$ Å^3[44] $< \alpha_{OH^-} = 2.03$ Å^3[51] $< \alpha_{CO_3^{2-}} = 3.85$ Å^3.[45] The OH^- anions are not particularly polarizable, but they tend to form Ln–O bonds that are shorter[52] than those of water.[53] In order to assess the influence exerted by these anions on the spectroscopic parameters of the lanthanide complexes, some comparisons were necessary. In the low temperature spectrum of the Eu^{3+} crystal, the $^7F_0 \rightarrow {}^5D_0$ band is located at 17258 cm^{-1}, whereas for the $Na_3[Eu(CO_3)_3]$ compound,[12] where Eu^{3+} is surrounded by 9 oxygen atoms from the carbonate anions, the band is located at 17234 cm^{-1}, which is in accordance with the general rule[46a,46b] that a larger accumulation of the total negative charge around Eu^{3+} brings about a lowering in the $^7F_0 \rightarrow {}^5D_0$ transition energy. Also, the $^7F_0 \rightarrow {}^5D_0$ band maximum for $[Eu(OH)_9]^{6-}$ in the $Eu(OH)_3$ crystal[54] (17225 cm^{-1} at 4.2 K) was shifted to lower energies in comparison to that of $[Eu(H_2O)_9]^{3+}$ in the crystalline $Eu(C_2H_5SO_4)_3\cdot 9H_2O$[55] (17256 cm^{-1} at 95 K). Hence, the substitution of the H_2O molecules by OH^- anions, where the C.N. and the symmetry of the surrounding for Eu^{3+} is preserved, brings about a 31 cm^{-1} shift to the lower energies. Similar changes were observed for the $^4I_{9/2} \rightarrow {}^2P_{1/2}$ transition in similar Nd^{3+} compounds. The $^4I_{9/2} \rightarrow {}^2P_{1/2}$ transition was shifted by 98 cm^{-1} to lower energies in $Nd(OH)_3$ (23272 cm^{-1} at 4 K)[56] compared to the same transition in $Nd(CF_3SO_3)_3\cdot 9H_2O$ (23370 cm^{-1} at 4 K).[57] The hydroxy anion is also capable of shortening the europium luminescence lifetime from 110 μs[47] in $Eu(C_2H_5SO_4)_3\cdot 9H_2O$ to 21 μs in $Eu(OH)_3$.[58]

We observed bathochromic shifts of the $^4I_{9/2} \rightarrow {}^2P_{1/2}$ (Nd^{3+}) and $^7F_0 \rightarrow {}^5D_0$ (Eu^{3+}) band maxima (23299 cm^{-1} for Nd^{3+} and 17252 cm^{-1} for Eu^{3+}) in the investigated solutions in comparison to those observed for the crystals at room temperature (23314 cm^{-1} for Nd^{3+} and 17276 cm^{-1} for Eu^{3+}). Other factors that should be considered are connected with the luminescent properties, namely, lifetimes (Eu and Tb complexes) and quantum yields (Eu complexes). The luminescence lifetime of Eu^{3+} in the crystal is longer than that in solution. Moreover, these values for the Eu^{3+}–carbonate complexes in H_2O and D_2O differ significantly. This suggested that around 1.5 ± 0.5 water molecule(s) are present in the first coordination sphere of Eu^{3+} but this is incompatible with the other spectroscopic results. These factors are more easily understood if the existence of a hydroxy complex is assumed. This may lead to the observed increase in the f–f transition intensities in solution, which in turn brings about an increase in the probability of the radiative processes and a shortening of the radiative luminescence lifetimes. Thus, the luminescence quantum yield is larger for the Eu^{3+}–carbonate complex in solution than it is in the crystal. Given that hydrolysis of the complex may occur in the aqueous solution under these conditions (pH ≈ 12), the presence of the $[Ln(CO_3)_4(OH)]^{6-}$ species is probable. This conclusion may be extended to the lanthanides that are lighter than Eu. On the other hand, the similarity between the luminescence lifetimes of the Tb carbonate complex in H_2O and D_2O excludes the presence of OH oscillators in the first coordination sphere of Tb^{3+} and points towards $[Tb(CO_3)_4]^{5-}$ as the main species in solution. The Stern–Volmer constants indicated that polynuclear species do not form in the solutions.

Thus, a comparison between the spectroscopic results obtained for the lanthanide carbonate complexes in the crystals and in the aqueous solutions enabled us to postulate that (1) the coordination environment of the metal ions for the heavy lanthanides (Dy–Lu) are similar in both of the phases, namely, $[Ln(CO_3)_4]^{5-}$ with an octacoordinate metal cation and bidentate carbonate anions, (2) a hydroxy nine-coordinate species, $[Ln(CO_3)_4(OH)]^{6-}$, forms for the light lanthanides (La–Eu), (3) terbium forms an octacoordinate $[Tb(CO_3)_4]^{5-}$ complex in solution and a nonacoordinate $[Tb(CO_3)_4(H_2O)]^{5-}$ complex in the crystalline state while no conclusions were drawn with regards to gadolinium, (4) the Stern–Volmer constants that were determined for the Tb^{3+} and Eu^{3+} complexes indicate that monomeric species dominate in the solutions.

Experimental Section

All of the chemicals used were analytical grade. The solutions of $LnCl_3$ were prepared from the appropriate lanthanide oxides, Pr_6O_{11} (99.9%), Nd_2O_3 (99.9%), Gd_2O_3 (99.9%), Tb_4O_7 (99.9%), Dy_2O_3 (99.9%), Ho_2O_3 (99.9%), Er_2O_3 (99.9%), Tm_2O_3 (99.9%), Lu_2O_3 (99.9%), and Y_2O_3 (99.9%), which were obtained from Merck, Sm_2O_3 (99.9%), Eu_2O_3 (99.99%), Yb_2O_3 (99.99%), which were obtained from Stanford Materials, and hydrochloric acid (POCH). The stock solutions of the Ln^{3+} chlorides were standardized with EDTA (POCH) by using Xylenol Orange (Merck) as the indicator.

The solutions of the Ln^{3+} carbonate complexes were prepared by mixing the $LnCl_3$ and K_2CO_3 stock solutions in appropriate molar ratios for the given spectroscopic measurements.

Crystal Preparation: An aqueous solution (20 mL) of $[C(NH_2)_3]_2CO_3$ (ABCR) (0.050 mol) was mixed with an aqueous solution (10 mL) of $LnCl_3$ (0.0025 mol). The solution was heated at 90 °C (±5 °C) under reflux until the initially formed precipitates dissolved. The final pH of the solutions was approximately 12. Large (5 to 15 mm of diameter) crystals of **I** and **II** were formed during the slow evaporation (a few months) of the water. The results of the elemental analyses of **I** and **II** are shown in Table 11.

Table 11. The elemental analysis of **I** ($H_{36}C_9N_{15}O_{15}Ln$) and **II** ($H_{34}C_9N_{15}O_{14}Ln$).

	H_{calc} (%)	H_{exp} (%)	C_{calc} (%)	C_{exp} (%)	N_{calc} (%)	N_{exp} (%)
I						
Pr	4.93	4.93	14.7	14.77	28.57	28.82
Nd	4.91	5.05	14.63	16.47	28.44	28.02
Sm	4.87	4.82	14.51	14.78	28.21	29.15
Eu	4.86	4.89	14.48	15.17	28.15	28.20
Gd	4.83	4.72	14.38	14.53	27.95	28.62
Tb	4.82	4.82	14.35	14.48	27.89	28.36
II						
Dy	4.64	4.75	14.63	14.41	28.43	27.79
Ho	4.62	4.85	14.58	14.29	28.34	27.95
Er	4.61	4.82	14.53	14.65	28.25	27.27
Tm	4.6	4.85	14.5	14.29	28.19	27.95
Yb	4.57	4.93	14.42	14.77	28.03	28.82
Lu	4.56	4.76	14.39	15.08	27.96	26.92
Y	5.15	5.45	16.25	16.35	31.58	32.41

Single-Crystal X-ray Diffraction Analysis: The appropriate crystals were cut from larger ones and were mounted on a Kuma KM4 diffractometer equipped with a CCD counter. The collected data were corrected for polarization, Lorentz, and absorption, the last of which was calculated from the crystal habits that were captured from the photo scans. The positions of Ln or Y were found from Patterson maps and the remainder of the non-H atoms were found from difference Fourier maps. The positions of the C-bonded hydrogen atoms were calculated geometrically. All of the water H atoms that could be found were refined freely. The refinements were full-matrix with all of the non-H atoms anisotropic. All of the computations were performed with the SHELXS97 and SHELXL97 programs.[59] The molecular graphics were prepared with DIAMOND.[60]

CCDC-800327 (for Pr), -800326 (for Nd), -800328 (for Sm), -800322 (for Eu), -800323 (for Gd), -800329 (for Tb), -800320 (for Dy), -800324 (for Ho), -800321 (for Er), -800330 (for Tm), -800331 (for Yb), -800325 (for Lu), -800332 (for Y) contain the supplementary crystallographic data for this paper. These data can be obtained free of charge from The Cambridge Crystallographic Data Centre via www.ccdc.cam.ac.uk/data_request/cif.

Theoretical Calculations: The DFT calculations for the complex anions were performed with the ADF suite of programs.[61] In the case of the $[Ln(CO_3)_4(H_2O)]^{5-}$ anions (**I**), it was necessary to optimize the O–H distances. The relevant Ln–O–H angles and the O′–

Ln–O–H torsion angles were kept frozen to prevent migration of the H atoms towards the neighbouring O atoms. The positions of the non-H atoms were kept as fixed input from the X-ray refinement. For the $[Ln(CO_3)_4]^{5-}$ anions (**II**), no geometry optimization was performed. The PW91 functional and the TZ2P basis, which was composed of double ζ functions for the core electrons, triple ζ for the valence ones and two polarization functions, were used; the core was not frozen. The scalar relativity was included by using the ZORA method and the bases scaled to ZORA, supplied with the ADF packet, were used. The natural bond orbital (NBO) analysis was performed with NBO 5.0.[62] The final calculations were unsuccessful for the **I** anions, therefore we decided to compute the properties for the hypothetical $[La(CO_3)_4(H_2O)]^{5-}$ anion with geometrical parameters that were taken from the Pr complex. The calculation for $[Yb(CO_3)_4]^{5-}$ also did not eventually converge. For comparison purposes we have calculated the properties of the CO_3^{2-} anion with the geometry optimized in vacuo.

Spectroscopic Measurements and Calculations

IR Spectroscopy: The IR spectra were recorded with a Bruker IF S66 spectrometer. The spectra of the crystalline complexes in KBr pellets and nujol suspension were recorded in the range of 50 to 4000 cm^{-1}, while the aqueous solutions (c_{Ln} = 0.200 M, $c_{K_2CO_3}$ = 2.4 M) were measured in a CaF_2 cuvette in the spectral range of 1100 to 4000 cm^{-1}.

UV/Vis/NIR Spectroscopy

The reflectance spectra of the lanthanide carbonates powders were recorded with a Cary 5 UV/Vis/NIR spectrophotometer at 298 K. The electronic absorption spectra were recorded with a Cary 500 UV/Vis/NIR spectrophotometer at 298 K for solutions and crystals and at 4.2 K for crystals. The experimental oscillator strengths (P) were determined by using the Equation (10):

$$P = \frac{4.33 \cdot 10^{-9}}{c \cdot d} \cdot \int_{\sigma_1}^{\sigma_2} A(\bar{\nu}) \mathrm{d}\bar{\nu} \tag{10}$$

where c is the concentration of the Ln^{3+} ion in M, d is the length of the optical path in cm, and $A(\bar{\nu})$ is the absorbance as the function of the wavenumber in cm^{-1}.

The values of the Ω_λ parameters were calculated from the least-squares fitting of the oscillator strengths that were computed from the Judd–Ofelt[33,34] relation (11):

$$P_{ED} = \frac{8\pi^2 m_e c \left(n^2+2\right)^2}{27h(2J+1)n} \bar{\nu} \sum_{\lambda=2,4,6} \Omega_\lambda \left\langle f^N \psi J \left\| U^{(\lambda)} \right\| f^N \psi' J' \right\rangle^2 \tag{11}$$

to the experimental ones. P_{ED} is the oscillator strength of the f–f transition, m_e is the electron mass, c is the velocity of light, h is Planck's constant, n is the refractive index (1.51 for crystals and 1.38 for solutions), J is the total quantum number of the ground state, $\bar{\nu}$ is the wavenumber of the band maximum, and $\langle f^N \psi J \| U^{(\lambda)} \| f^N \psi' J' \rangle$ is the reduced matrix element of the unit tensor operator $U^{(\lambda)}$.[63] The root-mean-square error was determined from Equation (12):

$$\mathrm{rms} = \sqrt{\frac{\sum_{i=n}^{n} (P_{exp} - P_{calc})^2}{n-3}} \tag{12}$$

Luminescence Spectroscopy

The corrected emission spectra were recorded with Edinburgh Instruments FLS 920 and Aminco 500 spectrofluorometer. The luminescence decay curves were detected with Edinburgh Instruments FLS 920 Spectrometer.

The quenching experiments (Stern–Volmer constants) were carried out by mixing appropriate quantities of the Tb^{3+} and Eu^{3+} complexes and K_2CO_3. The relevant concentrations of the Ln^{3+} cations are given in Table 10 ($c_{K_2CO_3}$ = 2.4 M, pH ≈ 12).

The emission spectra and lifetime measurements were recorded at the following conditions: λ_{exc} = 394 nm, λ_{em} = 617 nm (for Eu^{3+}), λ_{exc} = 368 nm, λ_{em} = 548 nm (for Tb^{3+}), and λ_{exc} = 352 nm, λ_{em} = 576 nm (for Dy^{3+}).

The luminescence quantum yields for solutions of the Eu^{3+}, Tb^{3+}, and Dy^{3+} complexes were determined relative to quinine sulfate in 0.5 M H_2SO_4 (Φ = 55%), fluoresceine in 0.1 M NaOH (Φ = 93%), or $[Ru(bpy)_3]Cl_3$ (Φ = 4.3%) by using the Equation (13):

$$Q_X = Q_S \cdot \frac{n_X^2}{n_S^2} \frac{\int_{\bar{\nu}_1}^{\bar{\nu}_2} I_X(\bar{\nu}) \mathrm{d}\bar{\nu}}{\int_{\bar{\nu}_1}^{\bar{\nu}_2} A_S(\bar{\nu}) \mathrm{d}\bar{\nu}} \cdot \frac{1 - 10^{-\varepsilon_S \cdot d \cdot c_S}}{1 - 10^{-\varepsilon_X \cdot d \cdot c_X}} \tag{13}$$

where Q stands for the quantum yield, n is the refractive index (n_X = 1.38, n_S = 1.33), the integrals were taken for the emission spectra corrected for the instrument response, ε is the molar absorption coefficient, c in the concentration, and d is the thickness of the cuvette (1 cm). The subscripts X and S stand for the sample and the standard, respectively. The pairs of the sample and the standard spectra used in the above equation were taken at the same instrument setting (slit widths, photomultiplier voltage, etc.). The slits were 2 nm for the excitation and 2 nm for the emission recording.

Supporting Information (see footnote on the first page of this article): Selected crystal data and structure refinements for **I** and **II**, oscillator strengths and the Ω_λ parameters of the f–f transitions for the lanthanide carbonates in the crystal and the solution states, reflectance spectra of **I** and **II**, absorption spectra of the lanthanide carbonate complexes in solution.

Acknowledgments

We would like to thank Prof. Krystyna Bukietyńska for helpful discussions. Density functional calculations were carried out at the Wrocław Centre for Networking and Supercomputing (http://www.wcss.wroc.pl), grant No. 58.

[1] S. P. Sinha in *Systematics and the Properties of the Lanthanides* (Ed.: S. P. Sinha), D. Reidel Publishing Company, Dortdrecht, Holland, **1983**, pp. 451–499.
[2] H. S. Sherry, J. A. Marinsky, *Inorg. Chem.* **1964**, *3*, 330–335.
[3] J. Dumonceau, S. Bigot, M. Treuil, J. Faucherre, F. Fromage, *Compt. Rend. C* **1979**, *288*, 415–425.
[4] a) R. R. Rao, A. Chatt, *J. Radioanal. Nucl. Chem.* **1988**, *124*, 211–225; b) X. Liu, R. H. Byrne, *Mar. Chem.* **1995**, *151*, 213–221; c) X. Liu, R. H. Byrne, *J. Solution Chem.* **1998**, *27*, 803–

815; d) Y.-R. Luo, R. H. Byrne, *Geochim. Cosmochim. Acta* **2004**, *68*, 691–699.
[5] T. Vercouter, P. Vitorge, N. Trigoulet, E. Giffaut, C. Moulin, *New J. Chem.* **2005**, *29*, 544–553.
[6] R. Nagaishi, T. Kimura, S. P. Sinha, *Mol. Phys.* **2003**, *101*, 1007–1014.
[7] D. L. Bond, D. L. Clark, R. J. Donohoe, J. C. Gordon, P. L. Gordon, D. W. Keogh, B. L. Scott, C. D. Tait, J. G. Watkin, *Eur. J. Inorg. Chem.* **2001**, 2921–2926.
[8] V. Philippini, T. Vercounter, J. Aupiais, S. Topin, C. Ambard, A. Chaussé, P. Vitorge, *Electrophoresis* **2008**, *29*, 2041–2050.
[9] V. Philippini, T. Vercouter, P. Vitorge, *J. Solution Chem.* **2010**, *39*, 747–769.
[10] D. E. Hobart, K. Samhoun, J. P. Young, V. E. Norvell, G. Mamantov, J. R. Peterson, *Inorg. Nucl. Chem. Lett.* **1980**, *16*, 321–328.
[11] W. J. Rohrbaugh, R. A. Jacobson, *Inorg. Chem.* **1974**, *13*, 2535–2539.
[12] N. Mercier, M. Leblanc, E. Antic-Fidancev, M. Lemaitre-Blaise, *J. Solid State Chem.* **1997**, *132*, 33–40.
[13] W. Runde, M. P. Neu, C. Van Pelt, B. L. Scott, *Inorg. Chem.* **2000**, *39*, 1050–1051.
[14] D. L. Bond, D. L. Clark, R. J. Donohoe, J. C. Gordon, P. L. Gordon, D. W. Keogh, B. L. Scott, C. D. Tait, J. G. Watkin, *J. Chem. Soc., Dalton Trans.* **2000**, 1975–1980.
[15] D. L. Bond, D. L. Clark, R. J. Donohoe, J. C. Gordon, P. L. Gordon, D. W. Keogh, B. L. Scott, C. D. Tait, J. G. Watkin, *Inorg. Chem.* **2000**, *39*, 3934–3937.
[16] M. O. Awaleh, A. Ben Ali, V. Maisonneuve, M. Leblanc, *J. Alloys Compd.* **2003**, *349*, 114–120.
[17] G. S. Goff, M. R. Cisneros, C. Kluk, K. Williamson, B. Scott, S. Reilly, W. G. Runde, *Inorg. Chem.* **2010**, *49*, 6558–6564.
[18] A. N. Christensen, *Acta Chem. Scand.* **1973**, *27*, 2973–2981.
[19] a) H. J. Kaltz, H. Seidel, *Z. Anorg. Allg. Chem.* **1980**, *465*, 92–108; b) A. Lossin, G. Meyer, *Z. Anorg. Allg. Chem.* **1993**, *619*, 2031–2037; c) I. Kutlu, H. J. Kalz, R. Wartchow, H. Ehrhardt, H. Seidel, G. Meyer, *Z. Anorg. Allg. Chem.* **1997**, *623*, 1753–1758.
[20] W.-J. Feng, G.-P. Zhou, Z.-B. Liu, Y. Xu, *Acta Crystallogr., Sect. E* **2007**, *63*, i174.
[21] H. Dexpert, P. Caro, *Mater. Res. Bull.* **1974**, *9*, 1577–1583.
[22] V. Philippini, T. Vercouter, A. Chausse, P. Vitorge, *J. Solid State Chem.* **2008**, *181*, 2143–2154.
[23] a) A. Mondry, P. Starynowicz, *Inorg. Chem.* **1997**, *36*, 1176–1180; b) A. Mondry, P. Starynowicz, *J. Chem. Soc., Dalton Trans.* **1998**, 859–863; c) A. Mondry, P. Starynowicz, *Eur. J. Inorg. Chem.* **2006**, 1859–1867; d) A. Mondry, R. Janicki, *Dalton Trans.* **2006**, 4702–4710; e) R. Janicki, P. Starynowicz, A. Mondry, *Eur. J. Inorg. Chem.* **2008**, 3075–3082.
[24] a) D. E. Henrie, G. R. Choppin, *J. Chem. Phys.* **1968**, *49*, 477–481; b) D. E. Henrie, *Mol. Phys.* **1974**, *28*, 415–421; c) Y. M. Poon, D. J. Newman, *J. Phys. C: Solid State Phys.* **1984**, *17*, 4319–4325; d) M. Atanasov, C. Daul, H. U. Güdel, T. A. Wesołowski, M. Zbiri, *Inorg. Chem.* **2005**, *44*, 2954–2963; e) L. Petit, A. Borel, C. Daul, P. Maldivi, C. Adamo, *Inorg. Chem.* **2006**, *45*, 7382–7388.
[25] J. M. Adams, R. W. H. Small, *Acta Crystallogr., Sect. B* **1974**, *30*, 2191–2193.
[26] R. F. W. Bader, *Atoms in Molecules: a Quantum Theory*, *The International Series of Monographs on Chemistry*, Oxford, Clarendon Press, **1990**.
[27] F. L. Hirshfeld, *Theor. Chim. Acta* **1977**, *44*, 129–138.
[28] A. E. Reed, L. A. Curtiss, F. Weinhold, *Chem. Rev.* **1988**, *88*, 899–926.
[29] J. Fujita, A. E. Martell, K. Nakamoto, *J. Chem. Phys.* **1962**, *36*, 339–345.
[30] J. A. Ladd, W. J. Orville-Thomas, B. C. Cox, *Spectrochim. Acta B* **1964**, *20*, 1771–1780.
[31] A. Mondry, K. Bukietyńska, *J. Alloys Compd.* **2004**, *374*, 27–31.
[32] H. McConnell, *J. Chem. Phys.* **1952**, *20*, 700–704.
[33] B. R. Judd, *Phys. Rev.* **1962**, *127*, 750–761.
[34] G. S. Ofelt, *J. Chem. Phys.* **1962**, *37*, 511–520.
[35] A. Mondry, K. Bukietyńska, *Mol. Phys.* **2003**, *101*, 923–934.
[36] a) S. F. Mason, G. E. Tranter, *Chem. Phys. Lett.* **1983**, *94*, 29–33; b) S. F. Mason, *Inorg. Chim. Acta* **1984**, *94*, 313–322; c) R. D. Peacock, *Struct. Bonding (Berlin)* **1975**, *22*, 83–219; d) S. F. Mason, *Struct. Bonding (Berlin)* **1980**, *39*, 43–79.
[37] a) C. K. Jørgensen, B. R. Judd, *Mol. Phys.* **1964**, *8*, 281–290; b) D. M. Gruen, C. W. DeKock, *J. Chem. Phys.* **1966**, *45*, 455–460.
[38] a) S. F. Mason, *Inorg. Chim. Acta* **1984**, *94*, 313–322; b) C. Görller-Walrand, K. Binnemans in *Handbook on the Physics and Chemistry of Rare Earths* (Eds.: K. A. Gschneidner, Jr., L. Eyring), Elsevier, **1998**, vol. 25, pp. 101–264.
[39] K. Bukietyńska, A. Mondry, T. Pham Ngoc, P. Starynowicz, *J. Alloys Compd.* **1995**, *225*, 52–54.
[40] a) S. Tanabe, T. Ohyagi, N. Soga, T. Hanada, *Phys. Rev. B* **1992**, *46*, 3305–3310; b) S. Tanabe, T. Hanada, T. Ohyagi, N. Soga, *Phys. Rev. B* **1993**, *48*, 10591–10594.
[41] a) S. F. Mason, R. D. Peacock, B. Stewart, *Chem. Phys. Lett.* **1974**, *29*, 149–153; b) R. D. Peacock, *Struct. Bonding (Berlin)* **1975**, *22*, 83–121; c) S. F. Mason, *Struct. Bonding (Berlin)* **1980**, *39*, 43–81; d) M. F. Reid, F. S. Richardson, *Chem. Phys. Lett.* **1983**, *95*, 501–506.
[42] a) A. Mondry, P. Starynowicz, *J. Alloys Compd.* **1995**, *225*, 367–371; b) A. Mondry, *Inorg. Chim. Acta* **1989**, *162*, 131–137.
[43] a) K. Binnemans, K. van Herck, C. Görller-Walrand, *Chem. Phys. Lett.* **1997**, *266*, 297–302; b) K. Bukietyńska, A. Mondry, *J. Alloys Compd.* **2001**, *323–324*, 150–154.
[44] J. W. Rohleder, *Ann. Soc. Chim. Polonorum* **1972**, *46*, 2089–2097.
[45] B. W. N. Lo, *J. Phys. Chem. Solids* **1973**, *34*, 513–520.
[46] a) M. Albin, W. D. Horrocks Jr., *Inorg. Chem.* **1985**, *24*, 895–900; b) S. T. Frey, W. D. Horrocks Jr., *Inorg. Chim. Acta* **1995**, *229*, 383–390; c) G. R. Choppin, Z. M. Wang, *Inorg. Chem.* **1997**, *36*, 249–252.
[47] W. D. Horrocks Jr., D. R. Sudnick, *J. Am. Chem. Soc.* **1979**, *101*, 334–340; a) W. D. Horrocks Jr., D. R. Sudnick, *Acc. Chem. Res.* **1981**, *14*, 384–392.
[48] T. Kimura, Y. Kato, *J. Alloys Compd.* **1995**, *225*, 284–287.
[49] M. H. V. Werts, R. T. F. Jukes, J. W. Verhoeven, *Phys. Chem. Chem. Phys.* **2002**, *4*, 1542–1548.
[50] a) H. G. Brittain, *Inorg. Chem.* **1978**, *17*, 2762–2766; b) H. G. Brittain, *Inorg. Chem.* **1979**, *18*, 1740–1745.
[51] R. D. Shannon, R. X. Fischer, *Phys. Rev. B* **2006**, *73*, 235111–1–235111–28.
[52] a) G. W. Beal, W. O. Milligan, H. A. Wolcott, *J. Inorg. Nucl. Chem.* **1977**, *39*, 65–70; b) D. F. Mullica, W. O. Milligan, G. W. Beal, *J. Inorg. Nucl. Chem.* **1979**, *41*, 525–532.
[53] R. E. Gerkin, W. J. Reppart, *Acta Crystallogr., Sect. C* **1984**, *40*, 781–786.
[54] R. L. Conet, R. Faulhabert, *J. Chem. Phys.* **1971**, *55*, 5198–5206.
[55] T. Ohoka, Y. Kato, *Bull. Chem. Soc. Jpn.* **1983**, *56*, 1289–1300.
[56] E. Antic-Fidancev, M. Lemaitre-Blaise, P. Caro, *New J. Chem.* **1987**, *11*, 467–472.
[57] J. R. Quagliano, G. W. Burdick, D. P. Glover-Fischer, F. S. Richardson, *Chem. Phys.* **1995**, *201*, 321–342.
[58] W. Runde, C. Van Pelta, P. G. Allen, *J. Alloys Compd.* **2000**, *303–304*, 182–190.
[59] a) G. M. Sheldrick, *SHELXS-97*, *Program for structure solution*, University of Göttingen, **1997**; b) G. M. Sheldrick, *SHELXL-97*, *Program for structure refinement*, University of Göttingen, **1997**.
[60] *DIAMOND-Visual Crystal Structure Information System*, CRYSTAL IMPACT, Postfach 1251, 53002 Bonn, Germany.
[61] E. J. Baerends, J. Autschbach, A. Bérces, C. Bo, P. M. Boerrigter, L. Cavallo, D. P. Chong, L. Deng, R. M. Dickson, D. E. Ellis, M. van Faassen, L. Fan, T. H. Fischer, C. Fonseca

Guerra, S. J. A. van Gisbergen, J. A. Groeneveld, O. V.Gritsenko, M. Grüning, F. E. Harris, P. van den Hoek, H. Jacobsen, L. Jensen, G. van Kessel, F. Kootstra, E. van Lenthe, D. A. McCormack, A. Michalak, V. P. Osinga, S. Patchkovskii, P. H. T. Philipsen, D. Post, C. C. Pye, W. Ravenek, P. Ros, P. R. T. Schipper, G. Schreckenbach, J. G. Snijders, M. Solà, M. Swart, D. Swerhone, G. te Velde, P. Vernooijs, L. Versluis, O. Visser, F. Wang, E. van Wezenbeek, G. Wiesenekker, S. K. Wolff, T. K. Woo, A. L. Yakovlev, T. Ziegler, *ADF2008.01, SCM, Theoretical Chemistry*, Vrije Universiteit, Amsterdam, The Netherlands, **2008** http://www.scm.com.

[62] E. D. Glendening, J. K. Badenhoop, A. E. Reed, J. E. Carpenter, J. A. Bohmann, C. M. Morales, F. Weinhold, *NBO 5.0.* Theoretical Chemistry Institute, University of Wisconsin, Madison, **2001**.

[63] a) W. T. Carnall, P. R. Fields, K. Rajnak, *J. Chem. Phys.* **1968**, *49*, 4412–4423; b) W. T. Carnall, P. R. Fields, K. Rajnak, *J. Chem. Phys.* **1968**, *49*, 4424–4442; c) W. T. Carnall, P. R. Fields, K. Rajnak, *J. Chem. Phys.* **1968**, *49*, 4443–4446.

Received: February 23, 2011
Published Online: July 18, 2011

